Chromosome Removal Via Cellular Fragmentation and Aneuploid Blastomere Exclusion in Primate Embryos

Brittany L. Daughtry[1,8], Jimi L. Rosenkrantz[2,8], Nathan H. Lazar[3], Suzanne S. Fei[9,10], Nash Redmayne[8], Kristof A. Torkenczy[2], Andrew Adey[2,4], Lina Gao[10], Byung Park[10], Kimberly A. Nevonen[4], Lucia Carbone[2-5,9*], and Shawn L. Chavez[6-9*]

[1]Department of Cell, Developmental & Cancer Biology; [2]Department of Molecular and Medical Genetics; [3]Department of Medical Informatics & Clinical Epidemiology, [4]Knight Cardiovascular Institute, [5]Department of Medicine, [6]Department and Physiology & Pharmacology, [7]Department of Obstetrics & Gynecology; Oregon Health & Science University School of Medicine; Portland, Oregon

[8]Division of Reproductive & Developmental Sciences; [9]Primate Genetics Section, [10]Biostatistics & Bioinformatics Core; Oregon National Primate Research Center; Beaverton, Oregon

*To whom correspondence should be addressed:

Shawn L. Chavez, Ph.D.
505 NW 185th Avenue
Beaverton, OR 97006
email: chavesh@ohsu.edu
phone: 503-346-5423
fax: 503-690-5563

Lucia Carbone, Ph.D.
3303 SW Bond Avenue
Portland, OR 97239
email: carbone@ohsu.edu
phone: 503 494-7342

Keywords: Aneuploidy, chromosome, embryo, fragmentation, IVF, micronuclei, pre-implantation, rhesus, single-cell, sequencing

ABSTRACT

A major contributor to *in vitro* fertilization failure and embryo loss is aneuploidy. Human pre-implantation embryos often sequester mis-segregated chromosomes into micronuclei during mitosis, while undergoing a process called cellular fragmentation. Using live-cell imaging, single-cell/fragment DNA-Sequencing, and confocal analyses, we demonstrate in a large number of rhesus embryos that aneuploidy, micronuclei, and cellular fragmentation dynamics is conserved between primates. We also determined that ~18% of fragmented embryos encapsulate whole or partial chromosomes within cellular fragments, which are either maternal or paternal in origin and undergo DNA damage. Additional findings of reciprocal chromosome segments, uniparental genome segregation, and mixoploidy support the prevalence of chromosome breakage and abnormal cytokinesis. Despite frequent chromosomal errors, we show that embryos can prevent incorporation of fragments and non-dividing blastomeres at the blastocyst stage. We propose that embryos respond to segregation errors by eliminating micronuclei via cellular fragmentation and select against aneuploid blastomeres to overcome chromosome instability.

The demand for human *in vitro* fertilization (IVF) increases each year, but success rates as measured by live birth(s) have remained only ~30-35% for decades (cdc.gov/art). One of the leading causes of IVF failure and embryo loss is the presence of unbalanced whole chromosome(s), or aneuploidy. Estimates of aneuploidy in IVF embryos via high-resolution techniques are 50-80%, including those from young, fertile couples and irrespective of stage[1-6]. Although difficult to ascertain, a similar efficiency (~30-35%) arises from natural human pregnancies, with up to 70% of spontaneous miscarriages diagnosed as aneuploid[7-10]. Chromosomal mis-segregation in oocytes during meiosis has long been considered the primary reason for aneuploidy, especially in cases of advanced maternal age. However, recent studies using comprehensive chromosome screening (CCS) of all blastomeres in cleavage-stage human embryos established that mitotic errors occur at an equal or greater frequency than meiotic errors and irrespective of maternal age[1,2,4,6,11,12]. Mitotic chromosome mis-segregation may not only lead to aneuploidy, but can also give rise to a mosaic embryo with different chromosomal copy number amongst cells. While classified as aneuploid, euploid-aneuploid mosaic embryos may still result in the birth of healthy offspring upon transfer, which suggests that corrective mechanisms exist to overcome chromosomal instability (CIN) during pre-implantation development[13-15].

Another determining factor for the capacity of an IVF embryo to successfully implant is the timing and degree of cellular fragmentation, whereby cytoplasmic bodies pinch off of blastomeres during cytokinesis[16,17]. Distinct from cell death-induced DNA fragmentation[18,19], cellular fragmentation also occurs naturally following *in vivo* human conceptions[20,21], and is not associated with maternal age[22]. We previously demonstrated that cellular fragments can contain chromosomal material and that mis-segregated chromosomes are encapsulated into micronuclei during mitotic divisions[4]. Chromosomes within somatic cell micronuclei display an increased propensity to undergo double-stranded breaks and structural rearrangements, which may be due to asynchrony in DNA replication timing between micronuclei and the primary nucleus[23]. A similar phenomenon has been proposed to occur in micronuclei of human embryos[24,25], but a recent report suggests that mouse embryonic micronuclei do not rejoin the primary nucleus and instead undergo perpetual unilateral inheritance[26]. Unlike humans, early cleavage-stage mouse embryos rarely exhibit micronuclei and cellular fragmentation even in sub-optimal culture conditions[4,26-28] and when micronuclei are induced experimentally mouse embryos undergo cell lysis rather than fragmentation[29]. Beginning at the morula stage, however, ~10% of mouse embryos have been shown to contain micronuclei, and a similar number appeared between *in vivo* and IVF-derived embryos[26]. This suggests that *in vitro* culture does not affect micronuclei formation and may explain why mouse embryos exhibit a considerably lower incidence of aneuploidy at ~1-4%[14,30-32].

Previous studies with rhesus macaque embryos using DNA-fluorescent *in situ* hybridization (DNA-FISH) probes to human chromosomes 13, 16, 18, X, and Y indicated that the inicidence of aneuploidy in rhesus embryos is more comparable to human than mouse[33-35]. Given that only a few chromosomes were analyzed by low-resolution techniques, however, the actual percentage of rhesus embryos carrying chromosomal aberrations was unknown. Here, we used single-cell DNA-Sequencing (scDNA-Seq) to establish the frequency of whole and segmental chromosomal errors in a large number of rhesus cleavage-stage embryos. By reconstructing the chromosomal content of every cell and fragment, we determined that whole and partial chromosomes lost from blastomeres are sequestered into cellular fragments and undergo DNA damage. Thus, we propose that mis-segregated chromosomes encapsulated within embryonic micronuclei not only persist or rejoin the primary nucleus, but may also be eliminated from the embryo upon cytoplasmic pinching of cellular fragments from blastomeres. We also show that cellular fragments and non-dividing aneuploid blastomeres can be excluded from blastocysts prior to hatching, which may serve as potential mechanisms to surpass CIN during primate pre-implantation development.

RESULTS

Strategy for assessing aneuploidy, micronuclei, and cellular fragmentation in rhesus embryos

To determine the aneuploidy frequency in rhesus cleavage-stage embryos, we developed an experimental approach utilizing scDNA-Seq and time-lapse monitoring (TLM) to non-invasively assess pre-implantation development (**Fig. 1a**). Mature metaphase (MII) oocytes underwent conventional IVF and presumed zygotes with two polar bodies and/or pronuclei were analyzed by TLM to measure the time intervals between mitotic divisions, the degree of cellular fragmentation (**Supplementary Movie 1**), and other parameters indicative of embryo chromosomal status. After ~24-96 hours, each cleavage-stage embryo (N=50) was disassembled into blastomeres, cellular fragments, and polar bodies if still present. Samples were individually isolated for chromosomal copy number variation (CNV) analysis and single nucleotide polymorphism (SNP) genotyping to determine the parental origin of chromosomes. Another subset of intact embryos between the zygote and blastocyst stage were fixed and subjected to multi-color confocal imaging to assess micronuclei formation and DNA sequestration by cellular fragments. An additional 132 rhesus embryos were allowed to proceed in development to evaluate embryonic arrest versus successful progression to the blastocyst stage.

Frequency of micronucleation and cellular fragmentation is conserved between primates

One of the hallmarks of imminent aneuploidy in somatic cells and human embryos is the appearance of micronuclei containing mis-segregated chromosomes[4,36,37], as well as cellular fragmentation in the latter, which we hypothesized

represents a response to chromosomal mis-segregation. Analogous to humans[16,17], we determined that >65% (N=129/196) of rhesus cleavage-stage embryos exhibit some degree of cellular fragmentation when evaluated at high magnification (**Supplementary Fig. 1a**). Upon fixation and immunolabeling with the nuclear envelope marker, LAMIN-B1, we showed that rhesus embryos contain micronuclei as early as the zygote (**Fig. 1b**) or 2-cell stage (**Fig. 1c**) and that the emergence of micronuclei is often concomitant with cellular fragmentation by the 2-cell stage (**Fig. 1d**). Some of these fragments encapsulate nuclear DNA positive for DAPI staining that is inconsistent with polar bodies, which contain condensed chromosomes and degenerate within 24 hours of formation[38]. While micronuclei did not appear until the 5- to 9-cell stage or later in certain embryos (**Fig. 1e**,**f**), we determined that the inner cell mass (ICM) of blastocysts might retain micronuclei (**Fig. 1g**). We also observed a condensed chromosome without nuclear envelope that was separate from the mitotic spindle (**Fig. 1e**) to suggest that mis-segregated chromosomes in embryonic micronuclei undergo condensation with nuclear envelope breakdown similar to chromosomes in primary nuclei.

Approach for chromosomal copy number calling in single embryonic cells

Following embryo disassembly into single cells and cellular fragments (**Supplementary Fig. 1b**), the DNA in each sample was amplified, labeled with custom barcodes, PCR-validated using adapter sequences, and pooled for multiplex sequencing. The average number of filtered and uniquely mapped sequencing reads in individual libraries was between 0.8 and 1.2 million (**Supplementary Table 1**). To determine CNV, we developed a bioinformatics pipeline that compares read counts in contiguous windows across the genome between embryonic samples and rhesus female euploid (42,XX) fibroblasts (**Supplementary Fig. 1c**) using a combination of Variable Non-Overlapping Windows and Circular Binary Segmentation (CBS) called VNOWC. Before applying this approach to embryos, the pipeline was trained and tested on rhesus male euploid (42,XY) cells (**Supplementary Fig. S1d**), as well as human fibroblasts carrying known aneuploidies (trisomy 21 or monosomy X), with low levels of karyotypic heterogeneity (**Supplementary Fig. 1e,f**). Our bioinformatics pipeline was able to successfully detect chromosome losses and gains in all rhesus and human fibroblast samples, including single cells (**Supplementary Fig. 1h**). We calculated the unexpected calls for whole and segmental aneuploidies depending on the number of mapped reads and determined that window sizes containing 4,000 reads produced high confidence CNV calling (**Supplementary Fig. 1i,j**). Since a recent scDNA-Seq study showed improved CNV calling when the data was intersected with a Hidden Markov Model (HMM)[39], we employed a second bioinformatics pipeline that utilized both CBS and HMM called CBS/HMM Intersect (CHI) to validate CNV calls. The majority of CNV calls were shared between methods (N=150/177; 84.7%) and discordant CNV calls detected between the VNOWC (N=18/177; 10.2%) and CHI (N=9/177; 5.1%) pipelines were primarily sub-chromosomal differences (**Supplementary Fig. 1k**). These discordant calls were further analyzed based on recently described criteria[40], and we conservatively estimated that the remaining chromosomes (N=27) in question were euploid.

Rhesus cleavage-stage embryos are often aneuploid or mosaic due to mitotic errors

Using the dual-pipeline bioinformatics strategy, we sequenced 472 individual samples from 50 whole rhesus cleavage-stage embryos up to the 14-cell stage (**Supplementary Table 2**), 49 of which contained amplifiable DNA in blastomeres as determined by high mitochondrial (mtDNA) read counts (**Fig. 2a**). This included a surprisingly large proportion of what was initially thought to be cellular fragments, but later confirmed to be polar bodies by SNP analysis (N=43/248; described below). Each blastomere or polar body was classified as euploid or aneuploid and the type of chromosomal error determined by the following criteria: (1) Meiotic errors were primarily identified by an aneuploid polar body and in the absence of polar bodies or presence of only one euploid polar body, it was considered meiotic if the same chromosome was affected in all sister blastomeres. (2) Mitotic errors were defined as different and/or reciprocal chromosome losses and gains between blastomeres with euploid polar bodies. (3) Chaotic aneuploidy was determined by greater than five randomly distributed chromosomes affected in one or more blastomeres as previously described[41]. Based on the above criteria, 38.7% (N=19/49) of the embryos were comprised of only euploid blastomeres with no whole chromosomal errors and 26.5% (N=13/49) of these embryos also did not contain segmental aneuploidy (**Fig. 2a, Supplementary Table 2**). In contrast, 73.5% (N=36/49) of the embryos contained at least one blastomere with whole and/or partial chromosome losses and gains. After combining embryos with whole and/or segmental aneuploidy, further analysis revealed that 40.8% (N=20/49) consisted of blastomeres that were all affected, whereas 32.7% (N=16/49) exhibited euploid-aneuploid mosaicism. While both polar bodies were obtained from only ~20% (N=10/49) of the embryos and primarily at the early cleavage stages, ~74% (N=31/42) of those isolated were euploid. Thus, we were able to confidently call the inheritance of meiotic errors in 25% (N=9/36) and the occurrence of solely mitotic errors in 41.7% (N=15/36) of embryos, with the remaining 33.3% (N=12/36) either incurring both types of errors or unknown due to the complexity of chromosomal mosaicism (**Supplementary Table 3**). The incidence of chaotic aneuploidy was 28.6% (N=14/49) and this appeared to be mostly confined to embryos fertilized by a particular sperm donor (N=11/14). Representative examples of genome-wide chromosomal CNV plots from embryos with euploid, mosaic, aneuploid, and/or chaotic aneuploid blastomeres are shown in **Supplementary Figure 2**.

Reciprocal sub-chromosomal deletions and duplications indicate chromosome breakage

Excluding chaotic samples, we then assessed the frequency of whole, segmental, and small sub-chromosomal (<15Mb) CNVs in the embryos (**Fig. 2b**). Chromosomes 1 and 2 were the most highly susceptible to aneuploidy due to DNA

breakage, while chromosome 19 experienced the greatest incidence of whole CIN. However, this chromosome is GC rich and when combined with scDNA-Seq as previously shown for human chromosome 19, whole chromosomal losses and gains are difficult to distinguish from large segmental CNVs[39]. In contrast, chromosome 20 (corresponding to chromosome 16 in humans)[42,43] was the least frequently affected by aneuploidy. Large segmental deletions, duplications, and amplifications were predominantly located at the outer portion of chromosomal arms (N=33/37) (**Fig. 2c**), indicating that chromosomal breakage likely occurs in rhesus embryos as described for human embryos[1]. A small proportion of embryos (16.7%; N=6/36) underwent unbalanced breaks, in which the reciprocal chromosome segments were found in a sister blastomere (**Fig. 2d**). We determined that several of these breakpoints localized near existing centromeres or an inactivated ancient centromere in the case of chromosome 18. The approximate location of breaks in chromosomes 10 and 14 aligned with corresponding fission or inversion evolutionary breakpoints, respectively, in the common primate ancestor[44].

Cellular fragments may encapsulate whole or partial chromosomes lost from blastomeres

Although reciprocal CNV was observed in some embryos, the majority of segmental chromosome losses were not detected in the other blastomeres. Based on our previous findings of chromosomal material in cellular fragments of human embryos[4], we postulated that the missing chromosome(s) had been sequestered during fragmentation. To test this, we sequenced 175 single fragments obtained from each fragmented rhesus embryo. We found one instance in which both copies of chromosome 9 and 12 lost from blastomeres were located in a cellular fragment from the same embryo (**Fig. 3a**). By similarly reconstructing the chromosomal content of each embryo via single-cell/-fragment DNA-Seq, we observed additional instances of individual, multiple, and/or partial chromosomes in the fragments of other embryos (**Fig. 3b**). Maternal versus paternal SNP genotyping analysis, which is described below, revealed that chromosome-containing cellular fragments (CCFs) originate from either the mother or father (**Fig. 3c**). There did not appear to be preferential sequestering of particular chromosomes, as both small and large chromosomes were affected and the partial chromosomes identified in fragments ranged in size from 6 to 85 megabases (**Fig. 3d**). Overall, we confirmed the presence of entire or portions of chromosomes in one or more cellular fragments in ~18% (N=8/45) of fragmented embryos, but only ~6.3% (N=11/175) of cellular fragments examined contained chromosomal material. In addition, 88% (N=7/8) of the embryos with CCFs were aneuploid to varying degrees and it should be noted that only one of three blastomeres isolated from the single euploid embryo successfully amplified for CNV analysis (**Fig. 3e**).

Chromosome-containing cellular fragments are susceptible to DNA breaks and damage

Based on findings of chromosomal segments in cellular fragments, we next sought to determine whether the CCFs were susceptible to DNA damage and rapid degradation once separated from the primary nucleus. To accomplish this, we immunostained fragmented cleavage-stage embryos with LAMIN-B1 and gamma-H2A.X (γ-H2A.X), a marker of DNA damage and double-stranded breaks[45]. Not only did we detect nuclear DNA positive for DAPI staining in cellular fragments of rhesus embryos (**Fig. 3f**), but these CCFs appeared to lack or have a disrupted nuclear envelope as previously described for somatic cell micronuclei[46]. While immunostaining for γ-H2A.X revealed distinct puncta in the micronuclei of blastomeres, multiple γ-H2A.X foci were also identified in the DNA of cellular fragments (**Fig. 3g**). By measuring γ-H2A.X fluorescence intensity in these embryos, we determined that DNA damage was markedly increased in CCFs compared to both primary nuclei and micronuclei (**Fig. 3h**). Since DNA degradation and double-stranded DNA breaks are not distinguishable by γ-H2A.X immunosignals, however, it is also possible that sub-chromosomal segments were initially sequestered into cellular fragments rather than the product of DNA degradation.

SNP analysis confirms polar body identity and reveals parental contribution to aneuploidy

It is generally accepted that polar bodies degenerate within 24 hours of extrusion from the oocyte or zygote[38], but we unexpectedly identified a large proportion of polar bodies originally thought to be cellular fragments in several embryos beyond the 2- to 4-cell stage (**Fig. 2a**). To validate their identity, we isolated DNA from each of the parents and performed whole-genome DNA-Seq (**Supplementary Table 4**) for comparison of maternal versus paternal SNPs in all embryonic samples (**Supplementary Table 5**). Although this sequencing approach prevented highly confident genotyping of individual SNPs, combining multiple SNPs across each chromosome provided greater assurance than each SNP alone. The proportion of maternal SNPs was significantly different ($p<1.88\times10^{-4}$, binomial test) from the expected 50%, with an average of 80% of SNPs in presumptive polar bodies identified as maternal in origin (**Fig. 4a**).

After confirming the identity of polar bodies, SNP genotyping was used to assess the parental origins of all chromosomes in each blastomere. While the majority of euploid embryos were biparental (76.9%; N=10/13), the SNP analysis showed that three of these embryos contained blastomeres with chromosomes that were entirely from the mother (**Fig. 4b**) and either gynogenetic (embryos 8 and 25) or digynic triploid (embryo 9). In contrast, only ~45% of the aneuploid embryos were biparental in origin (N=15/33) and the remaining embryos were gynogenetic (N=2/33), androgenetic (N=1/33), polyploid (N=11/33), or contained a mixture of uniparental, biparental, and triploid cells termed mixoploid (N=4/33) (**Fig. 4c**, **Supplementary Fig. 3, Supplementary Table 5**). Further analysis revealed at least one case of a paternally contributed meiotic error (embryo 15; chromosome 1 monosomy) and that the majority of triploid embryos were comprised

of two copies of maternal chromosomes and one copy of each paternal chromosome (**Fig. 4d**). By comparing the CCFs observed in **Figure 3e** to the embryos from which they arose via SNP genotyping, we determined that these embryos were biparental (N=1/8), gynogenetic (N=3/8), androgenetic (N=1/8), triploid (N=1/8), or mixoploid (N=2/8). This suggests that the type of chromosomal abnormality resulting in the production of CCFs from embryos ranges in complexity.

Multipolar divisions often lead to chromosome loss and chaotic aneuploidy

One feature shared by several (N=6/8) of the embryos with CCFs was multipolar divisions at the 1- or 2-cell stage detected by TLM (**Supplementary Movie 2**). Some multipolar zygotes were also noticeably speckled in appearance, which resembled multiple microtubule organizing centers (MTOCs) in mouse embryos with acentrosomal spindle assembly[47]. When we evaluated higher order mitotic divisions in all embryos, we discovered that while only one of the 15 embryos with multipolar divisions was euploid, the remaining embryos were chromosomally abnormal with chaotic aneuploidy being the most prevalent (N=8/15) (**Fig. 5a**). Moreover, almost every blastomere in these eight embryos exhibited chaotic aneuploidy as demonstrated by the example in **Figure 5b**. SNP analysis of parental ratios showed that multipolar divisions often result in a complex mixture of maternal and paternal chromosomes (**Fig. 5c**) and that all of the multipolar embryos with chaotic aneuploidy originated from the same sperm donor (**Supplementary Fig. 4**). In one of these embryos (**Fig. 5d**), we identified a loss of chromosomes 4, 8, and 16 in three blastomeres and the reciprocal copies in two other blastomeres from the same embryo (**Fig. 5e,f**). Based on the 3:1 chromosomal ratios, this indicates that chromosome mis-segregation likely occurred during the tripolar division observed at the zygote stage, which was propagated by subsequent bipolar divisions. However, the blastomeres with chromosomal gains also contained only a single copy of chromosome 19 (blastomere 5) and/or a complete loss of chromosome 15 (blastomeres 9 and 10). We detected these missing chromosomes in additional cells (blastomere 3, 7, and 8) that appeared unusual in shape and size upon disassembly. By employing SNP genotyping, we were able to determine that the loss of chromosome 15 and 19 in these blastomeres was due to a nondisjunction event. This is based on findings of only paternal chromosomes 15 and 19 in blastomeres 3, 7, and 8, and the corresponding maternal chromosomes in blastomeres 5, 9, and 10 as well as biparental contribution of these chromosomes in blastomeres 1, 2, and 4 (**Fig. 5g**), all of which is depicted in **Figure 5h**.

The first three mitotic divisions are predictive of rhesus embryo fate

Based on findings of multipolar divisions at the 1- to 2-cell stage and previous reports that the timing intervals of the first three mitotic divisions are predictive of human blastocyst formation and/or early ploidy status[4,48,49], we sought to determine if mitotic timing was similarly prognostic for rhesus pre-implantation development. Therefore, an additional 92 rhesus zygotes were monitored by TLM, but allowed to progress up to blastocyst stage (**Supplementary Movie 3**). While 42 of these embryos arrested prior to day 7, the remaining embryos reached the blastocyst stage with a blastocyst formation rate of ~54% (N=50/92). Of the 92 embryos, ~18.5% (17/92) underwent a multipolar division and ~88% (N=15/17) of those arrested following the abnormal division. The two multipolar embryos that still formed blastocysts exhibited a unique 1- to 4-cell symmetrical multipolar division without cellular fragmentation at the 1- or 2- cell stage. An examination of the average time intervals between the first three mitotic divisions in embryos that successfully reached the blastocyst stage was 35.15 ± 15.26 minutes (mins.), 9.33 ± 2.52 hours (hrs.), and 1.97 ± 2.32 hrs., respectively. In contrast, the arrested embryos exhibited longer mitotic timing intervals and/or large standard deviations with averages of 59.21 ± 50.49 mins., 8.80 ± 10.82 hrs., and 6.27 ± 5.84 hrs. We observed statistically significant differences ($p \leq 7.1 \times 10^{-4}$; Levene's test) in the variances of all three divisions, but the medians of only the 1st and 3rd mitotic division were significantly different ($p \leq 7.6 \times 10^{-4}$; Mann-Whitney test) between the two embryo groups (**Supplementary Fig. 5a**). When each embryo was graphed as a symbol in 2- and 3-dimensional (**Supplementary Fig. 5b**) parameter plots, the blastocysts clustered more tightly in a similar region of mitotic timing than the arrested embryos. Using these data, we constructed a prediction tree and determined that if the time to the 2nd division was ~6 to ~15 hrs., and the duration of the 1st division was less than ~40 mins., or the time between the 2nd and 3rd division was less than 0.375 hrs., then the embryo had a high probability of progressing to the blastocyst stage with ~86% accuracy, sensitivity, and specificity (**Supplementary Fig. 5c)**. In an independent test using 40 additional embryos, the decision tree predicted developmental fate with 80% accuracy (N=32/40). A similar type of analysis was performed to determine if the first three mitotic divisions with or without cellular fragmentation could predict abnormal chromosome number in embryos, but no statistical differences were found (data not shown). This is likely because most euploid embryos were collected at the 2-cell stage.

Non-dividing aneuploid blastomeres and fragments are excluded during blastocyst formation

Since ~54% of embryos formed blastocysts and only ~26.5% of cleavage-stage embryos were entirely euploid, we reasoned that a proportion of the blastocysts were aneuploid to some extent. We documented six embryos with excluded fragments and/or large blastomeres that ceased dividing at the 2- to 4-cell stage and persisted up to the blastocyst stage by TLM. These cellular fragments and non-dividing blastomeres appeared to be confined to the perivitelline space or blastocoel cavity during the morula-to-blastocyst transition, respectively (**Fig. 6a**). Two of the blastocysts with excluded blastomeres also underwent a 1- to 4-cell symmetrical cell division without cellular fragmentation at the 1- or 2- cell stage as mentioned above (**Supplementary Movie 4**). Upon immunostaining one of these blastocysts with LAMIN-B1 and γH2A.X, we observed a large bi-nucleated blastomere with extensive DNA damage indicated by intense γH2A.X accumulation (**Figure 6b**). Numerous DAPI-positive nuclei were also detected in the zona pellucida (ZP) of the embryo

that exhibited cellular fragment exclusion following hatching (**Fig. 6c**). While the fragments could be collected, it was difficult to separate excluded blastomeres from the embryo once the blastocoel cavity formed. Therefore, we identified three additional embryos with blastomere exclusion for a total of nine embryos and disassembled them prior to or during morula compaction. Once isolated, we performed scDNA-Seq and determined that the excluded blastomeres were highly chaotic with multiple chromosomal losses and gains (**Fig. 6d**). SNP genotyping showed that the chromosomes in excluded blastomeres had various maternal and paternal origins (**Fig. 6e**) and because these blastomeres never divided again or in certain cases later lysed, we propose that blastomere exclusion is one mechanism by which an embryo can select against aneuploid cells.

DISCUSSION

Established estimates of aneuploidy in human IVF embryos via whole-genome methods are 50-80% regardless of maternal age, fertility status, or stage[1,2,4-6,11,12] and largely contribute to embryo loss and pregnancy failure. This does not occur in mice, which typically exhibit ~80% blastocyst formation rates and require chemical induction to achieve an aneuploidy frequency similar to humans[14,50]. While ~70% of cleavage-stage bovine embryos have been shown to be aneuploid[51,52], all of the oocytes collected for these studies were immature and *in vitro* maturation (IVM) increases aneuploidy by itself[32]. More importantly, this is not the procedure used in >98% of human IVF cycles, whereby oocytes are matured *in vivo* for aspiration and then undergo IVF (cdc.art/gov). Using the *in vivo* maturation approach, we demonstrate by scDNA-Seq of each blastomere in cleavage-stage rhesus embryos that macaques also have a high incidence of aneuploidy. Upon examination of pregnancy success in the rhesus time-mated breeding colony at the Oregon National Primate Research Center during the same timeframe (November-May; 2013-2017) we determined that, of the confirmed ovulation and mating cases, only 26.5% (N=72/272) resulted in live birth to suggest a similar correlation between *in vitro* and *in vivo* conceptions. Besides aneuploidy, we also show that rhesus cleavage-stage embryos exhibit micronuclei formation, cellular fragmentation, and multipolar divisions at an equivalent frequency to human embryos[4,16,17,53-55], events that rarely occur in the mouse[4,26-28], as well as similar mitotic timing. Based on all of the above, we argue that the rhesus monkey represents a suitable surrogate for studying the effects of human embryonic aneuploidy on normal pre-implantation development (**Fig. 7a**).

Although cellular fragmentation is often associated with aneuploidy and we previously demonstrated that fragments may contain chromosomal material[4], this is the first study to show that whole and/or partial chromosomes lost from blastomeres are encapsulated within cellular fragments. Once separated from the primary nucleus, chromosomes within somatic cell micronuclei undergo DNA damage and double-stranded breaks[23,46]. Chromothripsis, whereby chromosomes are “shattered” and rearranged in a single catastrophic event, also arises as a result of DNA damage in somatic cell micronuclei[56]. The occurrence of chromothripsis in embryos has been suggested[24,25], but not yet confirmed, due to the depth of genome coverage and large insert size required to accurately detect structural variants by scDNA-Seq[57]. We did identify large segmental losses, duplications, and amplifications at the outer portion of chromosome arms in rhesus blastomeres, a finding that is supported by terminal chromosome imbalances and rearrangements in human embryos[1]. This was not observed in CCFs, however, which may be due to the apparent requirement that the damaged chromosome(s) within somatic cell micronuclei be exposed to normal nucleoplasm of the primary nucleus to undergo DNA repair and rearrangement[56]. Given that mis-segregated chromosomes can become encapsulated in cellular fragments rather than persist or rejoin with the primary nucleus in embryos, embryonic micronuclei might avoid the chromosomal rearrangement part of this process. However, based on extensive γH2A.X signals in CCFs and excluded blastomeres, we speculate that severely damaged DNA is eliminated from the embryo to prevent further propagation of highly unstable chromosomes (**Fig. 7b**). Additional sequencing and bioinformatics approaches are required to delineate if there are structural differences in the chromosomes from embryonic micronuclei, cellular fragments, and excluded blastomeres, the latter of which may be more susceptible to chromothripsis due to primary nucleus exposure. Findings from these studies may also inform the cancer field, especially since there are parallels between embryonic and somatic cell micronuclei and recent evidence that polyploid giant cancer cells represent the somatic equivalent of blastomeres[58].

Whether chromosome sequestration by cellular fragments and blastomere exclusion are attempts at embryonic rescue is difficult to ascertain, but there was a clear association between these two events and multipolar divisions. TLM has shown that ~12% of human zygotes undergo multipolar divisions[53] and are less likely to form blastocysts and implant than zygotes that exhibit a bipolar 1st mitotic division[54]. Ottolini *et al*. also recently found that multipolar divisions occurring later in development are highly correlated with human embryo arrest[55]. Almost all of the rhesus embryos with higher order divisions here arrested prior to forming blastocysts and the two embryos that did progress underwent a 1- to 4-cell symmetrical cell division without fragmentation. These two embryos also exhibited blastomere exclusion during the morula-to-blastocyst transition to suggest that multipolar divisions might provide a mechanism to overcome aneuploidy under certain circumstances (**Fig. 7c**). This is supported by findings that some of the embryos with higher order divisions were either euploid with adjacent empty blastomeres or chromosomally mosaic. The most prevalent type of chromosomal abnormality observed in multipolar embryos was chaotic aneuploidy and all of these embryos shared a common sperm donor. Because the centrosome for the first mitotic division(s) is paternally inherited in most mammalian species except rodents[59,60], this indicates that defective or supernumerary centrosomes from the sperm contributes to higher order

divisions. Polyploid embryos often exhibit supernumerary centriole pairs and multipolar spindles[61] and we did detect what appeared to be distinct MTOC puncta in some triploid zygotes that underwent a multipolar division. Since sperm are also responsible for the activation of oocytes during fertilization[62,63], premature oocyte activation might have also contributed to the higher order divisions observed in this study. Regardless of the mechanism(s), the relationship between multipolar divisions and the appearance of CCFs or excluded blastomeres requires more detailed investigation to determine if these events overcome or further potentiate CIN in pre- and post-implantation embryos.

One of the most intriguing findings from the SNP analysis was the identification of a few euploid and a relatively large proportion of aneuploid embryos with cells that were derived from only one parent. This phenomenon, called uniparental genome segregation, has been described in bovine embryos at the zygote stage using IVM oocytes and is thought to underlie mixoploidy[51,52]. To our knowledge, this is the first study to show that it also occurs in embryos using the more typical *in vivo* oocyte maturation approach for fertilization and beyond the zygote stage. While it is fairly well established that gynogenetic and androgenetic embryos can result from IVF, we speculate that a similar percentage of human embryos with uniparental origins has not been reported given that current pre-implantation genetic screening (PGS) methods do not examine parental origins of aneuploidy unless SNP arrays are used. However, SNP arrays are rarely employed by clinics for CNV analysis due to high rates of allele drop-out and the need to include parental DNA to interpret SNPs[64]. Because all zygotes appeared morphologically normal with two polar bodies and/or pronuclei here, we highly suggest that embryo biopsies incorporate SNP genotyping as well as TLM to document the dynamics of multipolar divisions, cellular fragmentation, and blastomere exclusion. These suggestions are based on recent findings that blastocysts with euploid-aneuploid mosaicism can still produce healthy offspring in both humans and mice and that mouse embryos without a sufficient number of normal blastomeres at the 8-cell stage are selectively eliminated during early post-implantation development[13,14]. Even though it is impossible to perform CNV analysis of all cells in embryos that will be transferred, we surmise that mosaic rhesus embryos containing a sufficient number of euploid blastomeres with chromosomes of biparental origins would have implanted into a receptive uterus and continued in development. Given that we detected micronuclei in the ICM of certain blastocysts, however, whether mosaic embryos survive may also depend on which lineage(s) the aneuploid blastomeres are allocated to and if there is lineage-specific selection against abnormal cells as shown for chemically-induced mouse embryos[14]. Future work is necessary to capture the formation and fate of micronuclei, CCFs, and excluded blastomeres in real-time and determine whether such events are a deliberate attempt at eliminating aberrant chromosomes and blastomeres from the embryo.

METHODS

Rhesus embryos

Controlled ovarian stimulations (COS) were performed on adult female rhesus macaques of average maternal age (9.2 $\pm$ 2.3 years old) as previously described[65]. Briefly, 30 IU of recombinant human follicular stimulating hormone (FSH; donated from Organon, Roseland, NJ) was intramuscularly (IM) injected twice daily in cycling females at the start of menses for six consecutive days. On days 7 and 8, 30 IU of both FSH and recombinant human luteinizing hormone (LH; donated from Al Partlow) were co-injected twice each day. When estradiol levels reached greater than 200 pg/ml, females were IM injected with 0.1 ml/kg of Antide (donated from the Salk Institute, La Jolla, CA) the following day to block circulating gonadotropin-releasing hormone (GnRH) and prevent an endogenous LH surge. Approximately 36 hours prior to follicle aspiration, a single dose (1,100 IU) of human chorionic gonadotropin (hCG; EMD Serono Ovidrel®, Rockland, MA) was IM injected to initiate oocyte maturation.

Laparoscopic follicular aspirations were aseptically conducted on anesthetized animals using suction to obtain cumulus-oocyte complexes (COCs) collected in Tyrode's albumin lactate pyruvate (TALP)-HEPES media with 0.3% bovine serum albumin (BSA; Sigma-Aldrich, St. Louis, MO) and 1% Heparin sodium salt solution. COCs were isolated from follicular aspirates and denuded by gentle micropipeting in TALP-HEPES media containing 0.3% BSA and 3% hyaluronidase (Sigma-Aldrich, St. Louis, MO). Metaphase I (MI) and MII oocytes were incubated in TALP plus 0.3% BSA media at 37°C with 5% CO_2 for 4-6 hours. To minimize variability between sperm donors, fresh semen was collected from only 1 of 4 adult male rhesus monkeys of average paternal age (9.4 $\pm$ 1.5 years old) the same day as oocyte retrieval for conventional IVF. Mature MII oocytes were fertilized in 100 µL drops of TALP complete media (0.3% BSA and 0.006% sodium pyruvate) with 20 x 10^6/ml “swim up” sperm further diluted 9:1 with activator solution [10.3mM caffeine (Sigma C-0750) and 10.2mM cAMP (Sigma D-0627) in saline] as previously described[66,67]. Following IVF at 37°C with 5% CO_2 for 14-16 hours, excess sperm were removed from the fertilized oocytes and visually assessed for two pronuclei and/or two polar bodies. Confirmed zygotes were transferred to custom Eeva™ 12-well polystyrene petri dishes (Progyny, Inc., San Francisco, CA; formerly Auxogyn, Inc.) and cultured in 100 µL of one-step commercial media supplemented with 10% serum protein (LifeGlobal, Guildford, CT) under mineral oil (Sage™, Trumbull, CT) at 37°C with 6% CO_2, 5% O_2 and 89% N_2. Media was changed every two days by transferring the embryos to a new imaging dish until collected for analysis. All animal procedures were performed under the direction and assistance of the veterinary staff and animal technicians in the Division of Comparative Medicine at Oregon National Primate Research Center (ONPRC). The collection and preparation of oocytes and sperm was performed according to the approved Institutional Animal Care and Use Committee (IACUC)

Assisted Reproductive Technologies (ART) Support Core protocol #0095 entitled, "Assisted Reproduction in Macaques."

Time-lapse imaging

Rhesus embryos were monitored with an Eeva™ darkfield 2.2.1 or bimodal (darkfield-brightfield) 2.3.5 time-lapse microscope system (Progyny, Inc., San Francisco, CA) as previously described[49]. The Eeva™ TLM systems were comprised of an inverted microscope with light-emitting diode illumination, 10X Olympus objective, auto-focus, and 5 megapixel CMOS digital camera, all of which fit into a small tri-gas incubator (Panasonic Healthcare, Japan). Embryos were imaged every 5 min. with a 0.6 second (sec.) exposure time for one day in the case of 2-cell embryos, 1-2 days for 4-cell embryos, 1-3 days for the 5- to 16-cell stage, and up to 7 days for blastocysts. Each image was time stamped with a frame number and all images compiled into an AVI movie using FIJI software version 2.0.0 (NIH, Bethesda, MD). The time intervals between the appearance of the 1st cleavage furrow to the end of the 1st cytokinesis, the beginning of the 2nd mitotic division, and the start of the 3rd mitotic division identified by cleavage furrows were manually recorded by three separate individuals and represented as an average. Other features such as cellular fragmentation, asymmetrical/multipolar division, and fragment/blastomere exclusion were also examined and recorded for each embryo. For multipolar divisions, the time intervals were generally zero and reflected 3-4 simultaneous cleavage furrows. The timing of the first three mitotic divisions in each embryo was plotted in 2- and 3-dimensional parameter plots using R Studio (R Foundation for Statistical Computing, Vienna, Austria) and MATLAB R2016a (Mathworks, Natick, MA). Statistical tests included Mann-Whitney test for differences in medians and Levene's test for differences in variance per parameter between embryo groups. The pruned decision tree was generated using R Studio.

Embryo disassembly

The zona pellucida (ZP) was removed from each embryo by a ~30 sec. exposure to warm Acidified Tyrode's Solution (EMD Millipore, Temecula, CA) and washed with Ca^{2+} and Mg^{2+}-free phosphate buffered saline (PBS). Cleavage-stage embryos were disaggregated into single cells, polar bodies, and cellular fragments if present with Quinn's advantage Ca^{2+} and Mg^{2+}-free medium with HEPES plus 10% human albumin (Sage™, Trumbull, CT) with or without brief exposure to warm 0.05% trypsin-EDTA (Thermo Fisher Scientific, Waltham, MA) as necessary. Each blastomere, polar body, and cellular fragment was washed three times with Ca^{2+} and Mg^{2+}-free PBS to reduce carry over from cellular debris or residual DNA and collected individually in ~2 µL of Ca^{2+} and Mg^{2+}-free PBS for transfer to a sterile Ultraflux™ PCR tube (GeneMate, VWR, Radnor, PA). All of the above was performed under a stereomicroscope equipped with a digital camera (Leica Microsystems, Buffalo Grove, IL), which has movie-making capabilities, to document the collection of every sample. Once tubed, samples were flash frozen on dry ice and stored at -80°C. Only embryos for which the disassembly process occurred effectively with no apparent loss of material were carried forward for library preparation and sequencing.

Somatic cells

Human B-lymphocytes (GM12878, Coriell Institute, Camden, NJ) were obtained and processed as previously described[40]. Female human skin fibroblasts from patients with Monosomy X or Trisomy 21 (GM10179 and AG05024, respectively, Coriell Institute, Camden, NJ) as well as karyotypically normal female and male rhesus skin fibroblasts (AG08312 and AG08305, respectively, Coriell Institute, Camden, NJ) were grown to 70% confluency in DMEM F12 medium (Gibco, Gaithersburg, MD) supplemented with 10% fetal bovine serum (FBS; Sigma-Aldrich, St. Louis, MO). Cells were incubated with warm 0.05% trypsin-EDTA for suspension and the trypsin inactivated with DMEM F12 medium plus 10% FBS. The cell suspension was serially diluted in Ca^{2+}/Mg^{2+}-Free PBS until single cells were detected in microdrops under the stereomicroscope. Individual cells were isolated in ~2 µL of Ca^{2+} and Mg^{2+}-free PBS and transferred to the low-retention PCR tubes, quick frozen on dry ice, and stored at -80°C until DNA library preparation. Karyotyping of the human and rhesus primary fibroblasts (N=50 metaphase spreads per cell line) was performed by the OHSU Research Cytogenetics Laboratory.

Parental DNA

Whole blood was collected in K_2EDTA vacutainer collection tubes (BD Diagnostics, Franklin Lakes, NJ) from the male and female rhesus macaques used to produce embryos in this study by the Colony Genetics Resource Core within the Primate Genetics Program at ONPRC. Parental DNA was extracted using the Gentra® Puregene® blood kit (Qiagen, Germantown, MD) according to the manufacturer's protocol. Extracted DNA was stored at -80°C for the construction of sequencing libraries.

DNA library preparation

Single blastomere, polar body, cellular fragment, and skin fibroblast samples underwent DNA extraction and whole genome amplification (WGA) using the PicoPLEX single-cell WGA Kit (Rubicon Genomics, Ann Arbor, MI) according to the manufacturer's instructions with slight modifications. The three-step, one-tube protocol applies a proprietary amplification process with quasi-random primers to assure the production of highly reproducible sequencing libraries. DNA was released from samples with cell extraction enzyme at 75°C for 10 min. and subsequently pre-amplified with PicoPLEX pre-amp enzyme and a primer mix via a 95°C hotstart for 2 min. and 12 cycles of gradient PCR. Pre-amplified DNA was further amplified with PicoPLEX amplification enzyme and 48 uniquely-indexed Illumina sequencing adapters

provided by the kit or custom adapters with indices designed by Andrew Adey's laboratory as previously described[40]. Adapter PCR amplification consisted of a 95°C hotstart for four min., four cycles of 95°C for 20 sec., 63°C for 25 sec., and 72°C for 40 sec. and seven cycles of 95°C for 20 sec. and 72°C for 55 sec. Libraries were quantified with a Qubit HS DNA kit (Life Technologies, Eugene, OR) and validated for sequencing by PCR amplification of the adaptor sequences using the PCR Primer Cocktail (Illumina TruSeq® kit, San Diego, CA) and visualized by 2% agarose gel electrophoresis. Only libraries with DNA quantities greater than the no-template controls were included in sequencing. 50 ng of DNA was prepared from each blastomere or fibroblast, 25 ng from polar bodies and CCFs, and 5 ng from samples with low to no detectable DNA after WGA and/or no DNA smear indicative of a positive library following gel electrophoresis. Pooled libraries were purified with AMPure® XP beads (Beckman Coulter, Indianapolis, IN) according to the PicoPLEX instructional manual. Purified pooled libraries were again quantified with a Qubit HS DNA kit and quality assessed by a 2200 TapeStation and/or a 2100 Bioanalyzer (both from Agilent, Santa Clara, CA).

Parental DNA samples (1 ug) were fragmented using the Diagenode Bioruptor Pico (Denville, NJ) for a 300-400 base pair (bp) size selection. The NEBNext® DNA Library Prep Master Mix Set and NEBNext Multiplex Oligos for Illumina (NEB, Ipswich, MA) were then used to generate whole-genome sequencing libraries for each sample following the manufacturer's protocol. The libraries were quantified with the Qubit High Sensitivity dsDNA Assay (Invitrogen) and size distribution assessed with a 2100 Bioanalyzer High Sensitivity DNA Analysis Kit (Agilent).

Multiplex DNA sequencing

Pooled libraries of individual blastomeres, polar bodies, and cellular fragments as well as single somatic cell libraries from skin fibroblasts and parental DNAs were sequenced on Illumina platforms according to the following scheme: rhesus single fibroblast female (42XX) control samples (N=5) were first sequenced on an Illumina MiSeq (San Diego, CA) using the 150bp paired-end protocol and generated a total of ~9.66×10^6 reads (~1.93×10^6 reads/sample). An additional 20 single fibroblasts were sequenced on an Illumina NextSeq 500 (San Diego, CA) using a 75-cycle kit with a modified single-end workflow that incorporated 14 dark cycles at the start of the first read prior to the imaged cycles. This excluded the quasi-random priming sequences that are G-rich and lack a fluorophore for the two-color chemistry utilized by the NextSeq platform during cluster assignment. From these cells, we generated a total of ~34.5×10^6 reads (~1.72×10^6 reads/sample). Based on the similar number of reads obtained per sample between the two protocols, we then sequenced pools of 17 and 48 embryonic samples on the Illumina MiSeq using the 150bp paired-end protocol and generated a total of ~30.7×10^6 reads (~1.81×10^6 reads/sample), and ~117×10^6 reads (~2.44×10^6 reads/sample), respectively. Using the custom designed indices described above, additional pools of 146 and 225 embryonic samples were sequenced on the Illumina NextSeq again using our custom 75bp single-end protocol and generated a total of ~258×10^6 reads (~1.77×10^6 reads/sample), and ~227×10^6 reads (~1.01×10^6 reads/cell line), respectively. A final pool of 81 embryonic samples was sequenced on the Illumina NextSeq using our custom 75bp paired-end protocol and generated a total of ~74.8×10^6 reads (~9.23×10^5 reads/sample).

Parental DNA multiplexed libraries were sequenced at the Oregon State University Center for Genomic Research and Biocomputing on the HiSeq 3000 platform using the 150 paired-end protocol for a total of 2.84×10^9 reads (1.56×10^8 reads/sample). One parental sample (ID: 26129) was sequenced on the Illumina NextSeq using our custom 75bp paired-end protocol for a total of ~3.50×10^8 reads.

All raw sample reads were de-multiplexed and sequencing quality assessed with FastQC as previously described[68]. Illumina adapters were removed from raw reads with the sequence grooming tool, Cutadapt[69], which trimmed 15 bases on the 5' end and five bases from the 3' end, resulting in reads of 120 bp on average. Trimmed reads were aligned to the most recent rhesus genome reference, RheMac8[70], using the BWA-mem option of the Burrows-Wheeler Alignment Tool[71] with default alignment parameters. To avoid read pile-ups due to common repeats, all repeat sequences were "masked" (converted to an "N") in the RheMac8 reference genome using Repeat Masker[72]. Resulting bam files were filtered to remove alignments with quality scores below 30 (Q<30) as well as alignment duplicates that were likely the result of PCR artifacts with the Samtools suite[73].

Copy number variant calling

Variable Non-Overlapping Window CBS (VNOWC)

Although PCR-based WGA is more effective for CNV analysis than isothermal amplification (non-PCR)-based techniques as previously shown[57], potential biases in read accumulation and dropout are expected to exist in individual samples from PicoPLEX WGA. To model the background rate of accumulation and dropout expected in a single-cell normal sample, five paired-end and twenty single-end sequenced rhesus 42XX fibroblast libraries were combined to form a paired-end and single-end reference, respectively. These reference samples were used to generate variable-sized windows with a constant number of expected reads per window (~4,000). The same windowing method was applied for reads from forty single human fibroblast samples. For each type of sample, we used the appropriate reference to calculate observed-to-expected ratios of read counts in each window given the total number of mapped reads. R package DNAcopy (version 1.44.0)[74] was used to perform circular binary segmentation (CBS) across each chromosome and identify putative copy

number changes between windows. Since the initial window ratios assume that reads are spread evenly across a euploid genome, a recalibration step was necessary to correct the expected number of reads given putative changes in copy number. Samples with mostly empty windows were presumed to have a base copy number of one, while samples with reads in the majority of windows were assumed to have a base copy number of two. The copy number estimates provided by CBS are rounded to the nearest integer and plotted, along with the corrected ratios for each window. A bioinformatics pipeline for calling chromosomal copy number was developed to implement the above steps (available at https://github.com/nathanlazar/Oocyte_CN). Findings from this custom CNV pipeline were validated with a secondary approach via Gingko (http://qb.cshl.edu/ginkgo), an open-source web tool for evaluating single-cell CNVs. To estimate false positive calls for the VNOWC pipeline, the human trisomy 21 and monosomy X reads from 10-cell karyotypically euploid fibroblasts were subsampled 100 times to levels typical of a single-cell sample (1M, 500K, 250K, and 100K reads). These subsampled reads were mapped to 4 different sets of window sizes (expecting 500, 1000, 2000, 4000 reads per window in controls) for a total of 3,200 CNV runs. Counts and standard deviations for unexpected whole and segmental CNVs greater than 15MBs were reported.

CBS/HMM Intersect (CHI)

A pipeline for GC bias correction, read normalization across both the genome and within each individual sample, and CNV calling was implemented as previously described[40]. Both the Hidden Markov Model (HMMcopy, version 3.3.0)[75] and Circular Binary Segmentation (DNAcopy, version 1.44.0)[74] packages were used to call CNVs based on parameters determined in Knouse et al.[39]. All calls from the HMM and CBS methods generated CNV profiles of variable sized windows that were intersected on a window-by-window basis.

Integration of VNOWC and CHI Pipelines

To optimize the accuracy of CNV calling, all samples were analyzed for whole/segmental chromosome losses and gains and small CNVs (<15 MB in length) by both the VNOWC and CHI methods. Shared CNV calls between the two methods were retained and discordant CNV calls for aneuploid whole or broken chromosomes were further examined. Chaotic aneuploid samples confirmed by both methods and discordant small CNV calls were not further analyzed. During the secondary assessment, the individual VNOWC chromosome plot of the discordant CNV call was first examined to determine if the call represented the integer loss or gain for the majority of estimated copy number points within the appropriate range of windows. Each smoothed, GC corrected individual chromosome HMM CNV plot from the CHI method was analyzed to determine if the majority of the Log2 transformed values were above 0.4 for a gain or below 0.35 for a loss. The smoothed, GC corrected individual chromosome CBS CNV plot from the CHI method was examined to determine if the majority of the Log2 transformed values were above 1.32 for a gain or below 0.6 for a loss. If two out of these three criteria were satisfied, the CNV call was retained or otherwise, a conservative assessment was made to categorize the chromosome in question as intact and euploid. Approximate DNA breakpoint locations were identified in rhesus chromosome ideograms adapted from Ventura et al.[76], http://www.biologia.uniba.it/macaque/, http://www.biologia.uniba.it/primates/2-OWM/MMU/MMU, and by identifying the syntenic g-band interval in the UCSC human assembly, hg38.

SNP parentage analysis

The whole genome reads from each parent and embryonic sample were processed using a pipeline following the best practice recommendations of the Broad Institute's Genome Analysis Toolkit (GATK)[77,78], but adapted for rhesus macaque. Briefly, reads were trimmed using Trimmomatic adaptive quality trimming[79] and aligned to the Mmul_8.0.1 reference genome using BWA-MEM[80]. BAM post-processing included local re-alignment around indels using GATK[78], and marking of duplicate reads using Picard tools (http://broadinstitute.github.io/picard). GATK's HaplotypeCaller was used to produce gVCF files for each parent and embryonic sample, followed by joint genotype calling using GenotypeGVCFs. Parent and embryonic samples were each joint genotyped as a separate set. SNPs located within repetitive regions that were identified using Repeat Masker (http://www.repeatmasker.org)[81] in parent samples were removed. The sequence data were managed and analyzed using DISCVR-Seq (Bimber, B., 2015; https://github.com/bbimber/discvr-seq/wiki), a LabKey Server-based system[82].

Due to low coverage scDNA-seq of the embryonic samples, many of the parental SNPs were observed in only one read per sample. To restrict the set of SNPs to only those of high confidence, we required that there be at least two reads for each SNP. We further selected only the SNPs for which the two parents contained opposite homozygous genotypes, meaning all reads matched one allele in one parent and the alternative allele in the other parent. While these restrictions reduced the number of usable SNPs per sample, it was more reliable and informative for determining parentage in the chromosomes of each blastomere, polar body, and CCF. The ratio of maternal to paternal SNPs was used to assess parental inheritance and overall ploidy for visualization by heat map via Morpheus (Broad Institute, Cambridge, MA) and histogram (MATLAB R2016a). Significance of SNP parental ratios was examined by cumulative binomial test with Bonferroni correction. All SNPs in CCF regions of interest were retained, whereas chromosomes in blastomeres and polar bodies that had fewer than 10 SNPs were removed to further increase confidence in calling parental inheritance.

Immunofluorescence confocal imaging

Embryos were placed in warmed acidified Tyrode's solution for 30 sec. to remove the ZP. ZP-free embryos were washed briefly in PBS-T, which consists of PBS (Invitrogen, Carlsbad, CA) with 0.1% BSA and 0.1% Tween-20 (Calbiochem, San Diego, CA). The embryos were fixed in 4% paraformaldehyde in PBS (Alfa Aesar, Ward Hill, MA) for 20 min. at room temperature (RT). Once fixed, the embryos were washed with gentle shaking three times for a total of 15 min. in PBS-T to remove any residual fixative. Embryos were permeabilized for antibody penetration in 1% Triton-X (Calbiochem, La Jolla, CA) for one hour at RT and then washed in PBS-T as described above. To block non-specific binding of the secondary antibody, embryos were transferred to a 7% donkey serum (Jackson ImmunoResearch Laboratories, Inc., West Grove, PA)/PBS-T solution overnight at 4°C and then washed in PBS-T as described above. For the visualization of LAMIN-B1 (ab16048, Abcam, Cambridge, MA) and γH2A.X (05-636, EMD Millipore, Temecula, CA), antibodies were diluted 1:1,000 and 1:100, respectively, in PBS-T with 1% donkey serum and the embryos sequentially stained overnight at 4°C. Between each antibody incubation, embryos were washed in PBS-T with gentle shaking four times for a total of 20 min. to ensure removal of non-specific antibody binding. Primary antibodies were detected using the appropriate species reactivity with 488- or 647-conjugated donkey Alexa Fluor secondary antibodies (Thermo Fisher Sci., Rockford, IL) at a 1:250 dilution in 1% donkey serum in PBS-T at RT for 1 hour in the dark. Embryos were then washed in PBS-T to remove non-specific antibody binding as described above. For nuclear DNA detection, embryos were stained with 1 mg/ml DAPI for 15 min. and then placed in a 30 μl drop of Global media with 10% protein under mineral oil on a glass bottom petri dish (Mattek, Ashland, MA). Immunofluorescence was visualized using a Leica SP5 AOBS spectral confocal system. Z-stacks 1-5 μM apart were sequentially imaged one fluorophore at a time to avoid spectral overlap between channels. Stacked images and individual channels for each color were combined for composite imaging files using the channel merger and z-projection functions in FIJI[83]. Mean fluorescence intensity of γ-H2A.X within nuclear structures was also measured for each stack in FIJI. In order to account for the potential loss of signal in distal optical sections of thick (>50μm) samples, the mean fluorescent intensities of multiple cytoplasmic regions were averaged and subtracted from the regions of interest to filter out background noise.

Quantification and Statistical Analysis

Significance of SNP parental ratios was examined using the cumulative binomial test with Bonferroni correction at $p<0.05$ (see above). Mann-Whitney test and Levene's test values for cell division parameters between arrested embryos and blastocysts were considered significant at $p<0.001$. Statistical analyses were performed using Microsoft Excel and R Studio.

Data and Software Availability

The sequencing data generated from this research has been deposited in the SRA under accession number SRP121351. The VNOWC bioinformatics pipeline for calling chromosomal copy number is available at https://github.com/nathanlazar/Oocyte_CN. Ginkgo, the tertiary single-cell CNV pipeline used in this study, can be found at http://qb.cshl.edu/ginkgo.

ACKNOWLEDGEMENTS

We are grateful to the ONPRC ART Core for their assistance with oocyte and sperm collection, Colony Genetics Resource Core for providing the parental DNA, Molecular & Cellular Biology Core for the Mi-Seq runs, Biostatistics and Bioinformatics Unit for the SNP analysis and TLM biostatistics, and Imaging & Morphology Core for confocal microscopy (supported by Grant S10 RR024585), all under the auspices of the NIH/OD ONPRC core grant (P51 OD011092). The TLM part of the study would not be possible without the generosity and support from Auxogyn, Inc. We also thank the OHSU ExaCloud Cluster Computational Resource, which allowed us to perform the intensive large-scale data workflows. We give special thanks to Drs. C. Bishop, C. Hanna, and J. Hennebold as well as C. Ramsey for rhesus samples and/or embryology expertise, S. Vitak and A. Fields for sequencing support, as well as G. Schau and M. Yan for assistance in CNV pipeline development. We also thank members of the Chavez and Carbone labs for insightful discussions. B.L.D. was supported by the P.E.O. Scholar Award, N.L. Tartar Research Fellowship, and T32 Reproductive Biology NIH Training Grant (T32 HD007133). J.L.R. was supported by the Collins Medical Trust Foundation and Glenn/AFAR Scholarship for Research in the Biology of Aging. N.H.L. was supported by a fellowship from the National Library of Medicine Biomedical Informatics Training Grant (T15LM007088). This work was supported by the NIH/NICHD (R01HD086073-A1), National Centers for Translational Research in Reproduction and Infertility (NCTRI) pilot funds (P50 HD071836), Howard & Georgeanna Jones Foundation for Reproductive Medicine, Medical Research Foundation of Oregon, and Collins Medical Trust (to SLC).

AUTHOR CONTRIBUTIONS

B.L.D. and S.L.C. designed the study, performed experiments, analyzed data, and wrote the manuscript. J.L.R. developed the single-cell library preparation and multiplex DNA-Seq approach. N.H.L. created and implemented the VNOWC CNV pipeline. S.S.F. aligned and genotyped the samples and generated SNP parentage summaries. N.R. performed TLM measurements and provided support for the embryology and imaging experiments. K.A.T. developed

and implemented the CHI CNV pipeline. A.A. provided single-cell sequencing expertise, the NextSeq runs, and human b-lymphocyte data. L.C. assisted in the study design and interpretation of the sequencing results. L.G. and B.P. provided biostatical analysis for the TLM and SNP data. K.N. prepared sequencing libraries from the parental DNA. All authors were involved in editing the manuscript.

COMPETING FINANCIAL INTERESTS

The authors declare no competing financial interests.

MATERIALS & CORRESPONDENCE

Further information and requests for resources and reagents should be directed to Shawn Chavez (chavesh@ohsu.edu).

REFERENCES

1. Vanneste, E. *et al.* Chromosome instability is common in human cleavage-stage embryos. *Nat Med* **15**, 577-583 (2009).

2. Chow, J. F. *et al.* Array comparative genomic hybridization analyses of all blastomeres of a cohort of embryos from young IVF patients revealed significant contribution of mitotic errors to embryo mosaicism at the cleavage stage. *Reprod Biol Endocrinol* **12**, 105 (2014).

3. Huang, J. *et al.* Validation of multiple annealing and looping-based amplification cycle sequencing for 24-chromosome aneuploidy screening of cleavage-stage embryos. *Fertil Steril* **102**, 1685-1691 (2014).

4. Chavez, S. L. *et al.* Dynamic blastomere behaviour reflects human embryo ploidy by the four-cell stage. *Nat Commun* **3**, 1251 (2012).

5. Minasi, M. G. *et al.* Correlation between aneuploidy, standard morphology evaluation and morphokinetic development in 1730 biopsied blastocysts: a consecutive case series study. *Hum Reprod* **31**, 2245-2254 (2016).

6. Johnson, D. S. *et al.* Preclinical validation of a microarray method for full molecular karyotyping of blastomeres in a 24-h protocol. *Hum Reprod* **25**, 1066-1075 (2010).

7. Ogasawara, M., Aoki, K., Okada, S. & Suzumori, K. Embryonic karyotype of abortuses in relation to the number of previous miscarriages. *Fertil Steril* **73**, 300-304 (2000).

8. Zinaman, M. J., Clegg, E. D., Brown, C. C., O'Connor, J. & Selevan, S. G. Estimates of human fertility and pregnancy loss. *Fertil Steril* **65**, 503-509 (1996).

9. Miller, J. F. *et al.* Fetal loss after implantation. A prospective study. *Lancet* **2**, 554-556 (1980).

10. Wilcox, A. J., Weinberg, C. R. & Baird, D. D. Timing of sexual intercourse in relation to ovulation. Effects on the probability of conception, survival of the pregnancy, and sex of the baby. *N Engl J Med* **333**, 1517-1521 (1995).

11. McCoy, R. C. *et al.* Common variants spanning PLK4 are associated with mitotic-origin aneuploidy in human embryos. *Science* **348**, 235-238 (2015).

12. Vanneste, E. *et al.* What next for preimplantation genetic screening? High mitotic chromosome instability rate provides the biological basis for the low success rate. *Hum Reprod* **24**, 2679-2682 (2009).

13. Greco, E., Minasi, M. G. & Fiorentino, F. Healthy Babies after Intrauterine Transfer of Mosaic Aneuploid Blastocysts. *N Engl J Med* **373**, 2089-2090 (2015).

14. Bolton, H. *et al.* Mouse model of chromosome mosaicism reveals lineage-specific depletion of aneuploid cells and normal developmental potential. *Nat Commun* **7**, 11165 (2016).

15. Fragouli, E. *et al.* Analysis of implantation and ongoing pregnancy rates following the transfer of mosaic diploid-aneuploid blastocysts. *Hum Genet* **136**, 805-819 (2017).

16. Antczak, M. & Van Blerkom, J. Temporal and spatial aspects of fragmentation in early human embryos: possible effects on developmental competence and association with the differential elimination of regulatory proteins from polarized domains. *Hum Reprod* **14**, 429-447 (1999).

17. Alikani, M. *et al.* Human embryo fragmentation in vitro and its implications for pregnancy and implantation. *Fertil Steril* **71**, 836-842 (1999).

18. Hardy, K. *et al.* From cell death to embryo arrest: mathematical models of human preimplantation embryo development. *Proc Natl Acad Sci USA* **98**, 1655-1660 (2001).

19. Xu, J., Cheung, T., Chan, S. T., Ho, P. & Yeung, W. S. The incidence of cytoplasmic fragmentation in mouse embryos in vitro is not affected by inhibition of caspase activity. *Fertil Steril* **75**, 986-991 (2001).

20. Buster, J. E. *et al.* Biologic and morphologic development of donated human ova recovered by nonsurgical uterine lavage. *Am J Obstet Gynecol* **153**, 211-217 (1985).

21. Pereda, J. & Croxatto, H. B. Ultrastructure of a seven-cell human embryo. *Biol Reprod* **18**, 481-489 (1978).

22. Wu, D. H. *et al.* Age does not influence the effect of embryo fragmentation on successful blastocyst development. *Fertil Steril* **95**, 2778-2780 (2011).

23. Crasta, K. *et al.* DNA breaks and chromosome pulverization from errors in mitosis. *Nature* **482**, 53-58 (2012).

24. Pellestor, F., Gatinois, V., Puechberty, J., Genevieve, D. & Lefort, G. Chromothripsis: potential origin in gametogenesis and preimplantation cell divisions. A review. *Fertil Steril* **102**, 1785-1796 (2014).

25. Pellestor, F. Chromothripsis: how does such a catastrophic event impact human reproduction? *Hum Reprod* **29**, 388-393 (2014).

26 Vazquez-Diez, C., Yamagata, K., Trivedi, S., Haverfield, J. & FitzHarris, G. Micronucleus formation causes perpetual unilateral chromosome inheritance in mouse embryos. *Proc Natl Acad Sci USA* **113**, 626-631 (2016).

27. Dozortsev, D., Ermilov, A., El-Mowafi, D. M. & Diamond, M. The impact of cellular fragmentation induced experimentally at different stages of mouse preimplantation development. *Hum Reprod* **13**, 1307-1311 (1998).

28. Winston, N. J. & Johnson, M. H. Can the mouse embryo provide a good model for the study of abnormal cellular development seen in human embryos? *Hum Reprod* **7**, 1291-1296 (1992).

29. Chavez, S. L. *et al.* Comparison of epigenetic mediator expression and function in mouse and human embryonic blastomeres. *Hum Mol Genet* **23**, 4970-4984 (2014).

30. Lightfoot, D. A., Kouznetsova, A., Mahdy, E., Wilbertz, J. & Hoog, C. The fate of mosaic aneuploid embryos during mouse development. *Dev Biol* **289**, 384-394 (2006).

31. Macaulay, I. C. *et al.* G&T-seq: parallel sequencing of single-cell genomes and transcriptomes. *Nat Methods* **12**, 519-522 (2015).

32. Treff, N. R. *et al.* Next Generation Sequencing-Based Comprehensive Chromosome Screening in Mouse Polar Bodies, Oocytes, and Embryos. *Biol Reprod* **94**, 76 (2016).

33. Dupont, C. *et al.* Incidence of chromosomal mosaicism in morphologically normal nonhuman primate preimplantation embryos. *Fertil Steril* **93**, 2545-2550 (2010).

34. Dupont, C., Froenicke, L., Lyons, L. A., Bavister, B. D. & Brenner, C. A. Chromosomal instability in rhesus macaque preimplantation embryos. *Fertil Steril* **91**, 1230-1237 (2009).

35. Dupont, C., Bavister, B. D., Armant, D. R. & Brenner, C. A. Rhesus macaque embryos derived from MI oocytes maturing after retrieval display high rates of chromosomal anomalies. *Hum Reprod* **24**, 929-935 (2009).

36. Cimini, D., Fioravanti, D., Salmon, E. D. & Degrassi, F. Merotelic kinetochore orientation versus chromosome mono-orientation in the origin of lagging chromosomes in human primary cells. *J Cell Sci* **115**, 507-515 (2002).

37. Cimini, D. *et al.* Merotelic kinetochore orientation is a major mechanism of aneuploidy in mitotic mammalian tissue cells. *J Cell Biol* **153**, 517-527 (2001).

38. Schmerler, S. & Wessel, G. M. Polar bodies--more a lack of understanding than a lack of respect. *Mol Reprod Dev* **78**, 3-8 (2011).

39. Knouse, K. A., Wu, J. & Amon, A. Assessment of megabase-scale somatic copy number variation using single-cell sequencing. *Genome Res* **26**, 376-384 (2016).

40. Vitak, S. A. *et al.* Sequencing thousands of single-cell genomes with combinatorial indexing. *Nat Methods* **14**, 302-308 (2017).

41. Delhanty, J. D., Harper, J. C., Ao, A., Handyside, A. H. & Winston, R. M. Multicolour FISH detects frequent chromosomal mosaicism and chaotic division in normal preimplantation embryos from fertile patients. *Hum Genet* **99**, 755-760 (1997).

42. Rogers, J. *et al.* An initial genetic linkage map of the rhesus macaque (Macaca mulatta) genome using human microsatellite loci. *Genomics* **87**, 30-38 (2006).

43. Wienberg, J., Stanyon, R., Jauch, A. & Cremer, T. Homologies in human and Macaca fuscata chromosomes revealed by in situ suppression hybridization with human chromosome specific DNA libraries. *Chromosoma* **101**, 265-270 (1992).

44. Ruiz-Herrera, A. Chromosomal Rearrangements in Primates. *eLS* (John Wiley & Sons, Ltd) 1-9 (2015).

45. Rogakou, E. P., Pilch, D. R., Orr, A. H., Ivanova, V. S. & Bonner, W. M. DNA double-stranded breaks induce histone H2AX phosphorylation on serine 139. *J Biol Chem* **273**, 5858-5868 (1998).

46. Hatch, E. M., Fischer, A. H., Deerinck, T. J. & Hetzer, M. W. Catastrophic nuclear envelope collapse in cancer cell micronuclei. *Cell* **154**, 47-60 (2013).

47. Courtois, A., Schuh, M., Ellenberg, J. & Hiiragi, T. The transition from meiotic to mitotic spindle assembly is gradual during early mammalian development. *J Cell Biol* **198**, 357-370 (2012).

48. Wong, C. C. *et al.* Non-invasive imaging of human embryos before embryonic genome activation predicts development to the blastocyst stage. *Nat Biotechnol* **28**, 1115-1121(2010).

49. Vera-Rodriguez, M., Chavez, S. L., Rubio, C., Reijo Pera, R. A. & Simon, C. Prediction model for aneuploidy in early human embryo development revealed by single-cell analysis. *Nat Commun* **6**, 7601 (2015).

50. Alper, M. M., Brinsden, P., Fischer, R. & Wikland, M. To blastocyst or not to blastocyst? That is the question. *Hum Reprod* **16**, 617-619 (2001).

51. Destouni, A. *et al.* Zygotes segregate entire parental genomes in distinct blastomere lineages causing cleavage-stage chimerism and mixoploidy. *Genome Res* **26**, 567-578 (2016).

52. Tsuiko, O. *et al.* Genome stability of bovine in vivo-conceived cleavage-stage embryos is higher compared to in vitro-produced embryos. *Hum Reprod* **32**, 2348-2357 (2017).

53. Chamayou, S. *et al.* The use of morphokinetic parameters to select all embryos with full capacity to implant. *J Assist Reprod Genet* **30**, 703-710 (2013).

54. Hlinka, D. *et al.* Time-lapse cleavage rating predicts human embryo viability. *Physiol Res* **61**, 513-525 (2012).

55. Ottolini, C. S. *et al.* Tripolar mitosis and partitioning of the genome arrests human preimplantation development in vitro. *Sci Rep* **7**, 9744 (2017).

56. Wu, L. *et al.* Full-length single-cell RNA-seq applied to a viral human cancer: applications to HPV expression and splicing analysis in HeLa S3 cells. *Gigascience* **4**, 51 (2015).

57. de Bourcy, C. F. *et al.* A quantitative comparison of single-cell whole genome amplification methods. *PLoS One* **9**, e105585 (2014).

58. Niu, N., Mercado-Uribe, I. & Liu, J. Dedifferentiation into blastomere-like cancer stem cells via formation of polyploid giant cancer cells. *Oncogene* **36**, 4887-4900 (2017).

59. Sathananthan, A. H. *et al.* Centrioles in the beginning of human development. *Proc Natl Acad Sci USA* **88**, 4806-4810 (1991).

60. Schatten, G., Simerly, C. & Schatten, H. Maternal inheritance of centrosomes in mammals? Studies on parthenogenesis and polyspermy in mice. *Proc Natl Acad Sci USA* **88**, 6785-6789 (1991).

61. Kalatova, B., Jesenska, R., Hlinka, D. & Dudas, M. Tripolar mitosis in human cells and embryos: occurrence, pathophysiology and medical implications. *Acta Histochem* **117**, 111-125 (2015).

62. Whitaker, M. Calcium at fertilization and in early development. *Physiol Rev* **86**, 25-88 (2006).

63. Yoon, S. Y. *et al.* Human sperm devoid of PLC, zeta 1 fail to induce Ca(2+) release and are unable to initiate the first step of embryo development. *J Clin Invest* **118**, 3671-3681 (2008).

64. McCoy, R. C. *et al.* Evidence of Selection against Complex Mitotic-Origin Aneuploidy during Preimplantation Development. *PLoS Genet* **11**, e1005601 (2015).

65. Stouffer, R. L. & Zelinski-Wooten, M. B. Overriding follicle selection in controlled ovarian stimulation protocols: quality vs quantity. *Reprod Biol Endocrinol* **2**, 32 (2004).

66. Wolf, D. P., Thomson, J. A., Zelinski-Wooten, M. B. & Stouffer, R. L. In vitro fertilization-embryo transfer in nonhuman primates: the technique and its applications. *Mol Reprod Dev* **27**, 261-280 (1990).

67. Lanzendorf, S. E., Gliessman, P. M., Archibong, A. E., Alexander, M. & Wolf, D. P. Collection and quality of rhesus monkey semen. *Mol Reprod Dev* **25**, 61-66 (1990).

68. Krueger, F., Andrews, S. R. & Osborne, C. S. Large scale loss of data in low-diversity illumina sequencing libraries can be recovered by deferred cluster calling. *PLoS One* **6**, e16607 (2011).

69. Chen, C., Khaleel, S. S., Huang, H. & Wu, C. H. Software for pre-processing Illumina next-generation sequencing short read sequences. *Source Code Biol Med* **9**, 8 (2014).

70. Zimin, A. V. *et al.* A new rhesus macaque assembly and annotation for next-generation sequencing analyses. *Biol Direct* **9**, 20 (2014).

71. Salavert Torres, J. *et al.* Using GPUs for the exact alignment of short-read genetic sequences by means of the Burrows-Wheeler transform. *IEEE/ACM Trans Comput Biol Bioinform* **9**, 1245-1256 (2012).

72. Tarailo-Graovac, M. & Chen, N. Using RepeatMasker to identify repetitive elements in genomic sequences. *Curr Protoc Bioinformatics* **4**, Unit 4 10 (2009).

73. Ramirez-Gonzalez, R. H., Bonnal, R., Caccamo, M. & Maclean, D. Bio-samtools: Ruby bindings for SAMtools, a library for accessing BAM files containing high-throughput sequence alignments. *Source Code Biol Med* **7**, 6 (2012).

74. Olshen, A. B., Venkatraman, E. S., Lucito, R. & Wigler, M. Circular binary segmentation for the analysis of array-based DNA copy number data. *Biostatistics* **5**, 557-572 (2004).

75. Ha, G. *et al.* Integrative analysis of genome-wide loss of heterozygosity and monoallelic expression at nucleotide resolution reveals disrupted pathways in triple-negative breast cancer. *Genome Res* **22**, 1995-2007 (2012).

76. Ventura, M. *et al.* Evolutionary formation of new centromeres in macaque. *Science* **316**, 243-246 (2007).

77. Van der Auwera, G. A. *et al.* From FastQ data to high confidence variant calls: the Genome Analysis Toolkit best practices pipeline. *Curr Protoc Bioinformatics* **43**, 11-33 (2013).

78. McKenna, A. *et al.* The Genome Analysis Toolkit: a MapReduce framework for analyzing next-generation DNA sequencing data. *Genome Res* **20**, 1297-1303 (2010).

79. Bolger, A. M., Lohse, M. & Usadel, B. Trimmomatic: a flexible trimmer for Illumina sequence data. *Bioinformatics* **30**, 2114-2120 (2014).

80. Li, H. & Durbin, R. Fast and accurate long-read alignment with Burrows-Wheeler transform. *Bioinformatics* **26**, 589-595 (2010).

81. Smit, A., Hubley, R. & Green, P. *RepeatMasker Open-4.0*. <http://www.repeatmasker.org> (2013-2015).

82. Nelson, E. K. *et al.* LabKey Server: an open source platform for scientific data integration, analysis and collaboration. *BMC Bioinformatics* **12**, 71 (2011).

83. Schindelin, J. *et al.* Fiji: an open-source platform for biological-image analysis. *Nat Methods* **9**, 676-682 (2012).

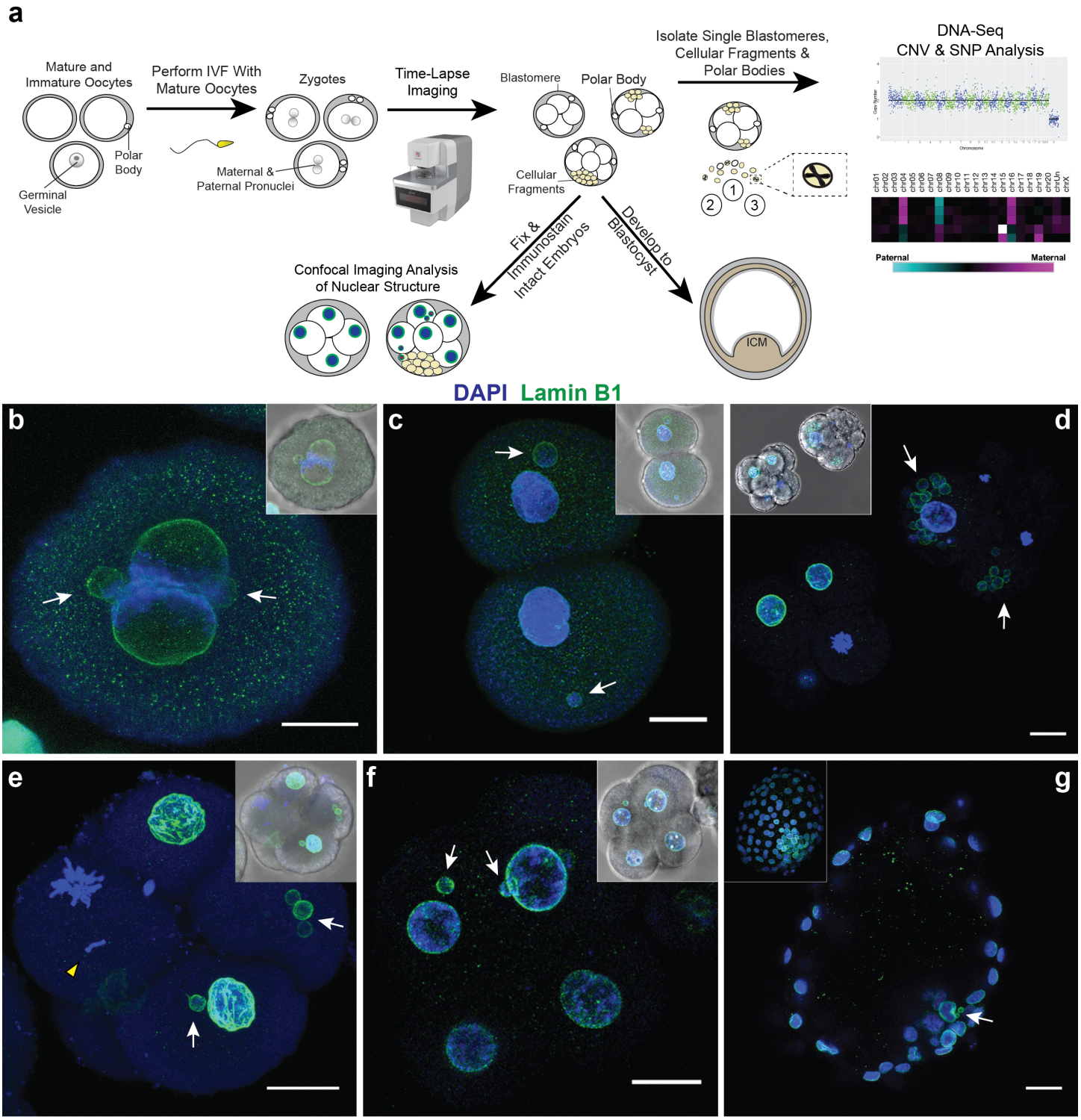

Figure 1. Approach for assessing CNV, micronuclei, and fragmentation dynamics in rhesus embryos. (a) Mature and immature oocytes were obtained from reproductive-age female rhesus macaques undergoing controlled ovarian stimulations. MII oocytes displaying one polar body were fertilized by conventional IVF with sperm from reproductive-age males. Early mitotic divisions of presumptive zygotes identified by two pronuclei and/or polar bodies were analyzed by time-lapse imaging. Cleavage-stage embryos were disassembled into individual blastomeres, cellular fragments, and/or polar bodies and analyzed by scDNA-Seq for CNV and SNP assessment. A subset of intact cleavage-stage embryos were fixed and immunostained for confocal imaging, while an additional group of embryos were cultured up to the blastocyst stage. **(b)** A zygote undergoing syngamy with two micronuclei (white arrows) using the nuclear envelope marker, LAMIN-B1 (green), and DAPI (blue) for nuclear DNA. **(c)** 2-cell embryo with one micronucleus in each blastomere. **(d)** Comparison of a fragmented (white arrowheads) 2-cell embryo with multiple micronuclei (right) and a non-fragmented 7-cell embryo (left). Single imaging plane of a Z-stacked **(e)** 5-cell embryo with a mis-segregated chromosome

(yellow arrowhead) and micronuclei as well as a **(f)** 9-cell embryo exhibiting micronuclei in two blastomeres, but no visible cellular fragmentation. Insets show a brightfield image for reference. Scale bars: 25 μm. **(g)** Blastocyst with at least two micronuclei in the ICM; the inset shows the maximum intensity projection of the embryo.

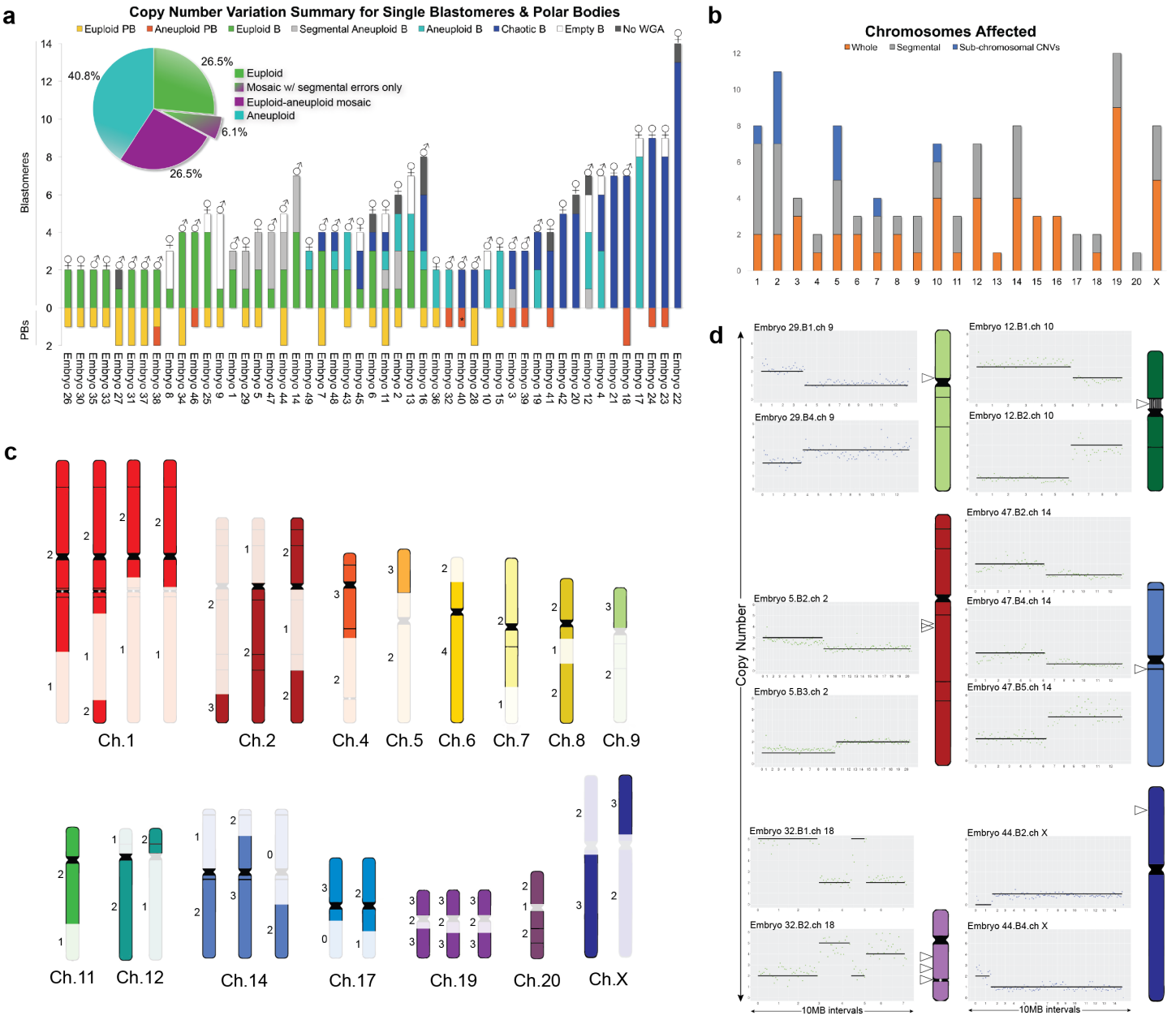

Figure 2. Assessment of whole and sub-chromosomal imbalances in single blastomeres and polar bodies. (a) CNV summary of rhesus embryos (N=49) from the 2- to 14-cell stage analyzed by scDNA-Seq. Stacked bars represent euploid (yellow) and aneuploid (orange) polar bodies; euploid (green), aneuploid (light blue), segmental-only aneuploid (purple), and chaotic aneuploid (dark blue) blastomeres; no WGA (gray); and empty blastomeres (white) detectable by mtDNA, but no genomic DNA reads. N=254 samples. Polar body classified as aneuploid containing only broken chromosomes labeled with asterisk (*). ♂: Y chromosome present ♀: Only X chromosome(s) present. Percentage of euploid, aneuploid, or mosaic embryos with euploid and aneuploid blastomeres is shown in upper left corner. (**b**) Number of times chromosomes were affected by whole (orange) or segmental (gray) gains or losses per non-chaotic aneuploid embryo. Small sub-chromosomal CNVs (<15MB) shown in blue. **(c)** Location of chromosomal breaks in embryos with segmental aneuploidy. Numbers to left of each chromosome represent the blastomere copy number state. (**d**) CNV plots of six embryos, in which chromosomal breakage resulted in a reciprocal loss and gain of chromosome segments between blastomeres (left). Rhesus chromosome ideograms showing the approximate breakpoint locations (right; white arrowheads) with horizontal lines representing conserved breakpoints between human and rhesus syntenic regions. Vertical lines in chromosome 10 delineate the nucleolus organizer region adjacent to the centromere and the gray circle in chromosome 18 designates the ancestral inactivated centromere. B, blastomere; PB, polar body; ch, chromosome.

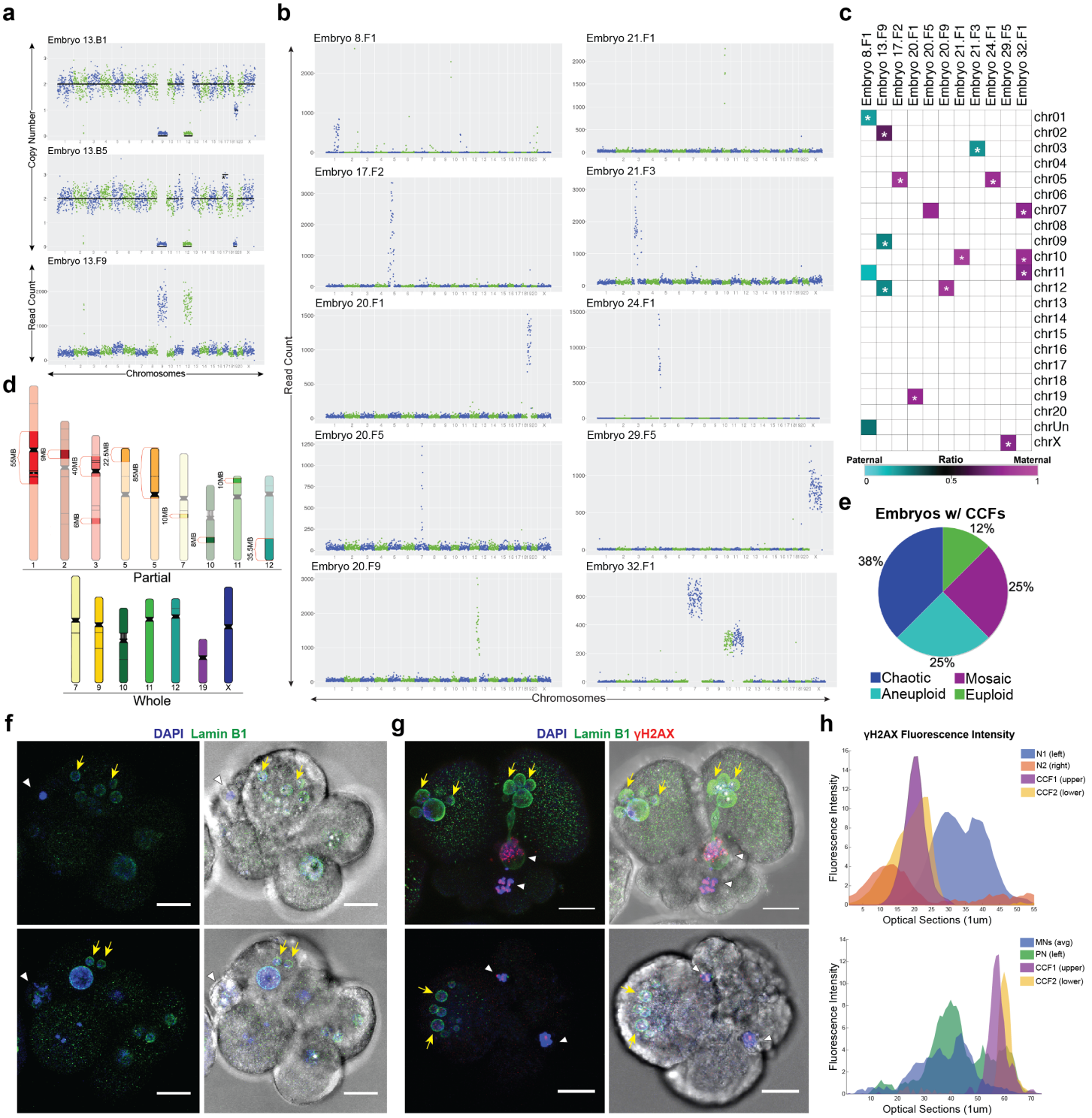

Figure 3. Micronuclei containing damaged chromosomes are eliminated via cellular fragmentation. (a) CNV plots demonstrating that chromosomes 9 and 12 lost from two blastomeres (top and middle; also missing 1-2 copies of chromosome 19) were detected in a cellular fragment (bottom) from the same embryo. **(b)** Additional examples of individual, multiple, and/or partial chromosomes in the cellular fragments of different rhesus embryos. **(c)** Heat map of maternal versus paternal SNP genotyping ratios showing that CCFs can originate from either the mother or the father. White asterisk (*) demarcates significant p-values ($p<9.1X10^{-6}$) for cumulative binomial test with Bonferroni correction. **(d)** Rhesus ideograms representing the whole (bottom) and partial chromosomes with approximate sizes highlighted that were detected in cellular fragments. **(e)** Percent of embryos with CCFs (N=8 embryos) that were chaotic (blue), aneuploid (turquoise), mosaic (magenta), and euploid (green). **(f)** 8-cell and 7-cell (bottom) embryo with CCFs (white arrowheads) identified by DAPI (blue) signals that are similar in size to the LAMIN-B1 (green) positive micronuclei (yellow arrows) in

adjacent blastomeres (left). Brightfield image (right) provided for reference. Scale bar: 25 μm. (**g)** 2-cell embryos (bottom is the same embryo in Figure 1D left) with multiple cellular fragments and micronuclei also immunostained for the double-stranded DNA break marker, γH2A.X (red), shows that the chromosomes within fragments are unstable and damaged. (**h**) γ-H2A.X fluorescence intensity measurements of primary nuclei (N or PN), micronuclei (MN), and chromosomes within cellular fragments (CCFs) for embryos to the immediate left.

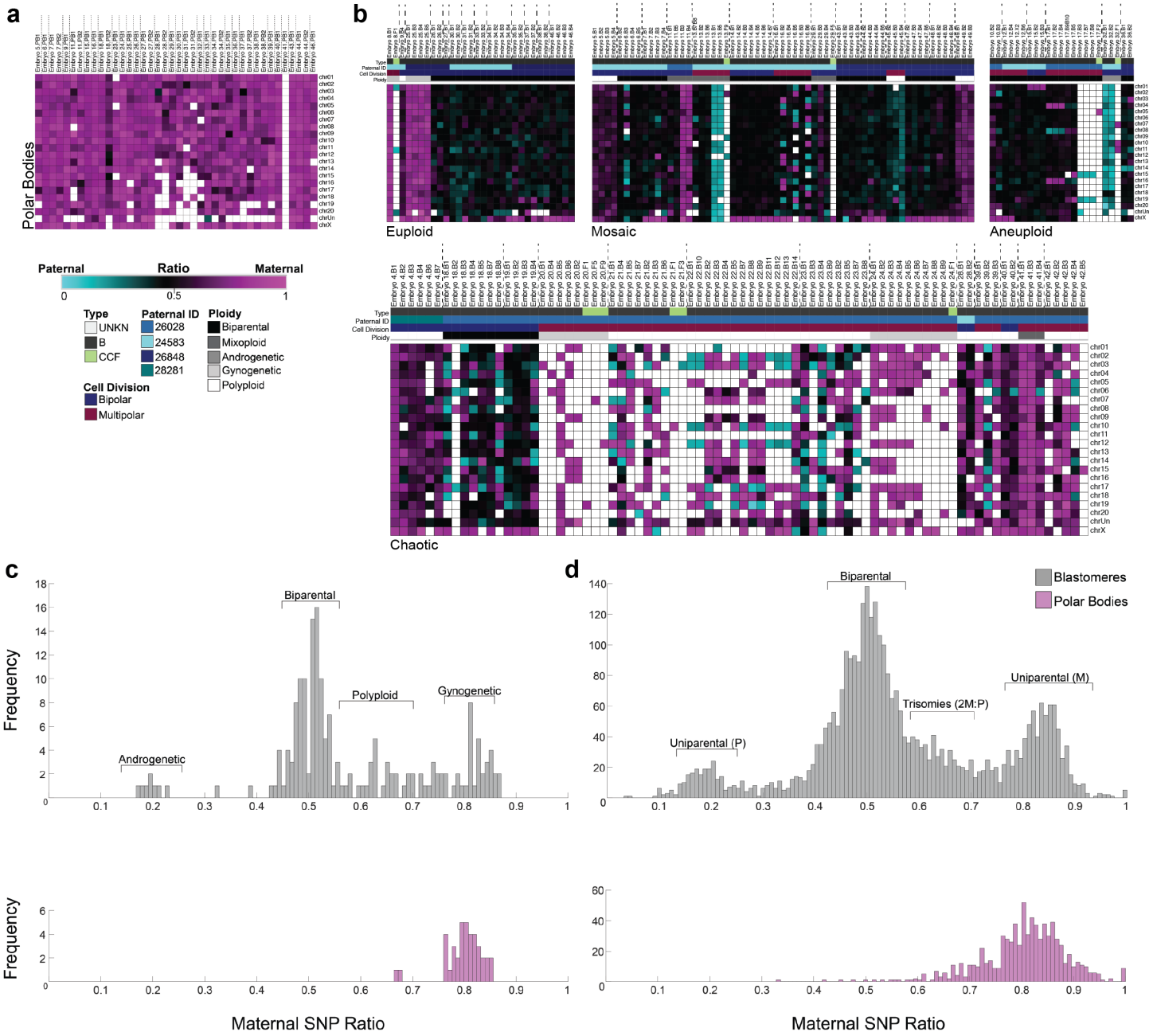

Figure 4. SNP profiling confirms polar bodies and reveals the complexity in parental contribution to aneuploidy. **(a)** Heat map of the SNP parentage ratios in presumptive polar bodies confirming their maternal origins and **(b)** of euploid, aneuploid, a mixture of euploid and aneuploid blastomeres (mosaic), or chaotic aneuploid embryos. Each embryo is separated by vertical dotted lines. Samples were further sorted based on the paternal donor, cell type, mitotic divisions, and whole embryo ploidy. Pink, blue, and black boxes indicate maternal, paternal, and biparental inheritance, respectively. White boxes show that either the chromosome was not detected or it could not be called with high confidence. **(c)** Histograms showing the distribution of SNP ratios across blastomeres (dark gray) and polar bodies (pink) in each sample revealed that the majority of rhesus embryos were biparental, but a small proportion were androgenetic, polyploid, or gynogenetic. **(d)** Frequency of SNPs ratios in histograms further stratified at an individual chromosome level.

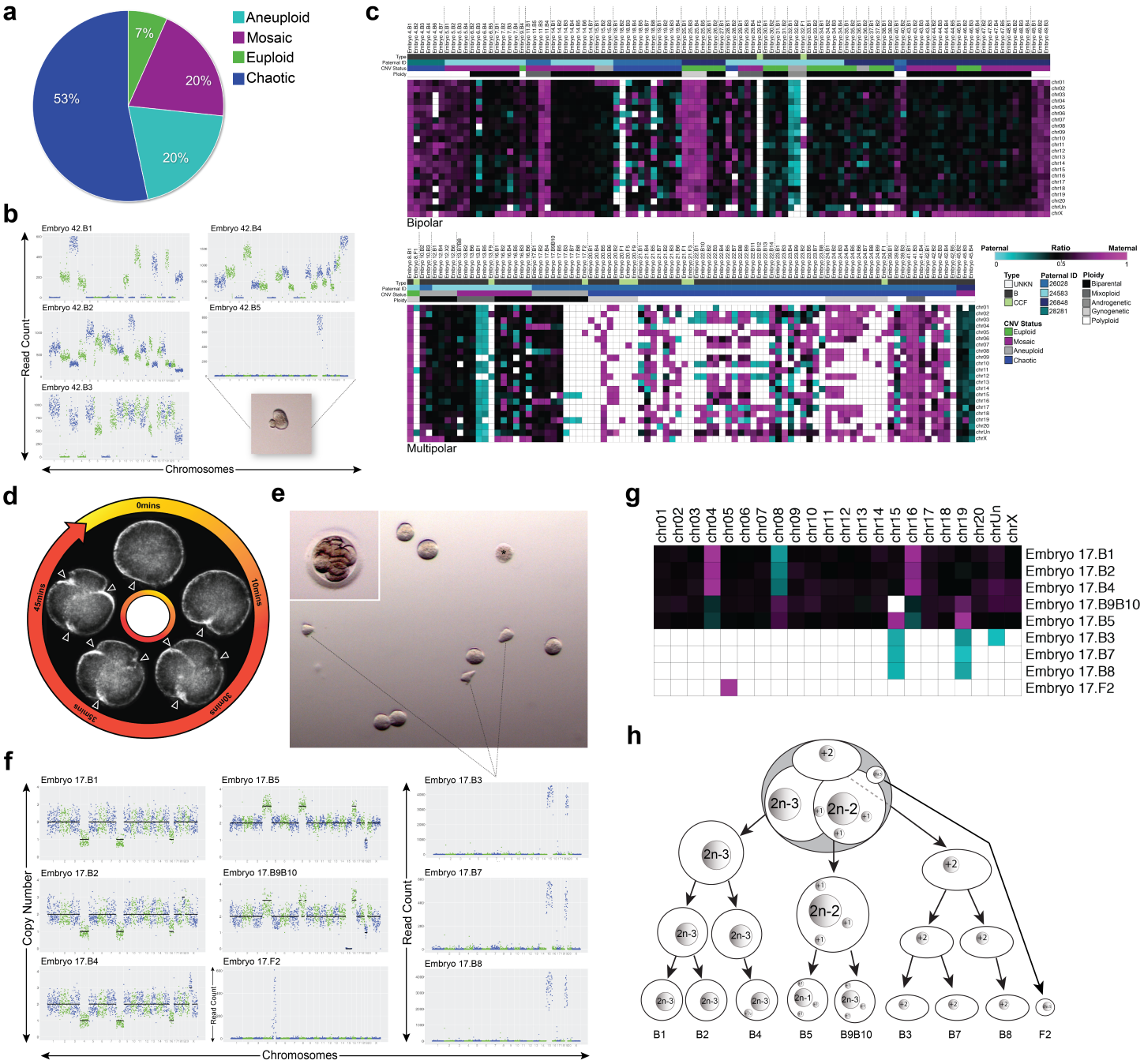

Figure 5. Multipolar divisions in embryos often result in chromosome loss and chaotic aneuploidy. (a) Ploidy status of rhesus embryos (N=15) with at least one multipolar division at the 1- or 2-cell stage. **(b)** CNV plots of blastomeres from an embryo, which underwent a multipolar 1st division, showing chaotic aneuploidy in almost every cell. Inset is a stereomicroscope image of blastomere 5 containing only chromosome 15 with a cellular fragment-like protrusion. **(c)** Heat map of SNP parentage ratios in embryos that underwent bipolar or multipolar cleavage(s) during the first three cell divisions. **(d)** Darkfield time-lapse images of a zygote undergoing a tripolar division. Arrowheads point to three simultaneous cleavage furrows. **(e)** Stereomicroscope image of the same embryo still intact (inset) and then disassembled. Blastomere 6 lysed and is demarcated with an asterisk (*). **(f)** The CNV plots of all whole blastomeres from the embryo showing multiple reciprocal chromosome losses and gains. Dotted lines indicate irregularly shaped blastomeres that each contained only two chromosomes. **(g)** Heat map of maternal versus paternal SNP ratios for this embryo delineates parental inheritance. **(h)** Hypothetical schematic of the chromosome copy number state for each blastomere in this embryo based on the imaging and CNV analysis.

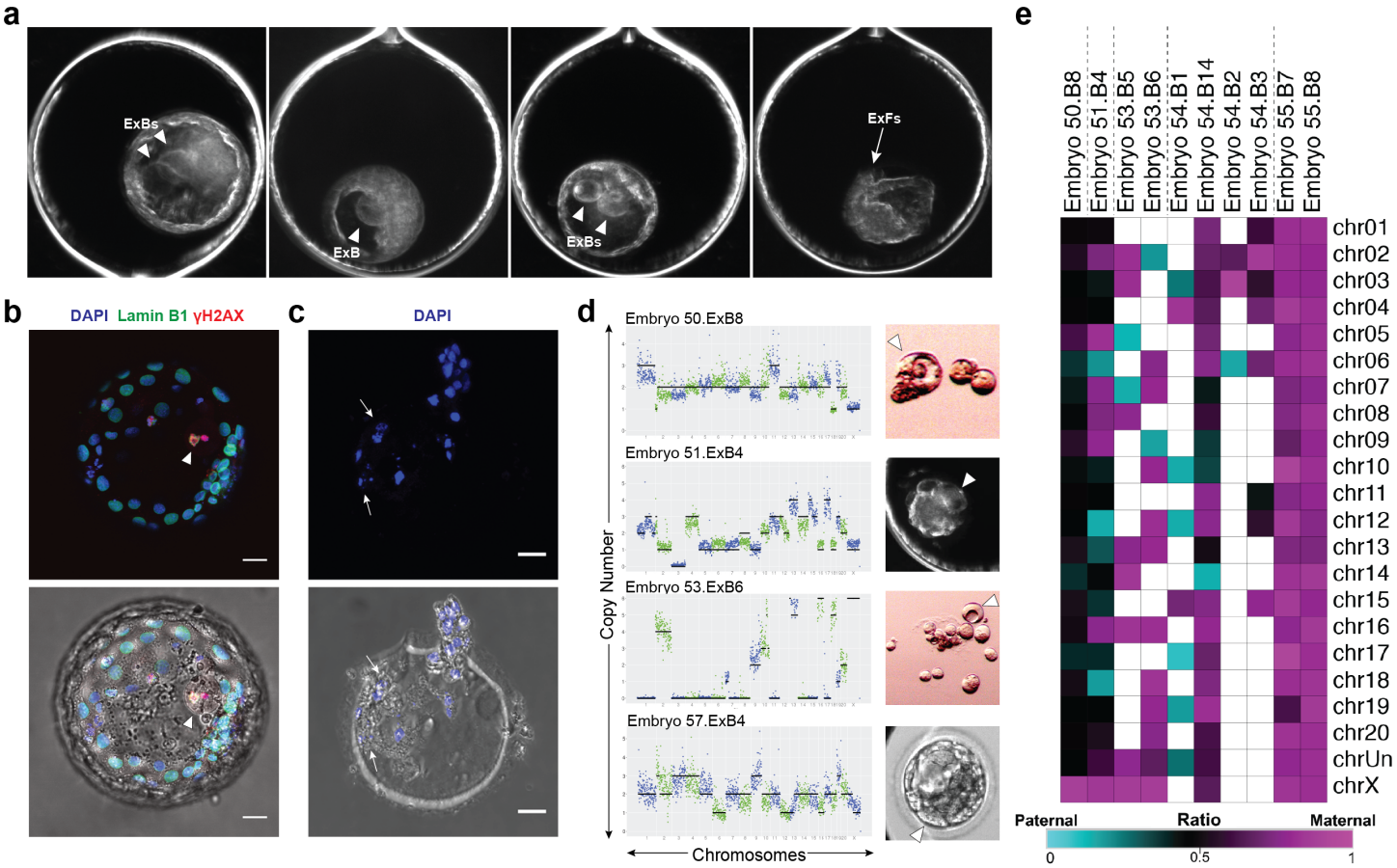

Figure 6. Cellular fragments and aneuploid blastomeres are excluded upon blastocyst formation. **(a)** Darkfield time-lapse image frames from four rhesus blastocysts exhibiting exclusion of either 1-2 non-dividing blastomeres confined to the blastocoel cavity (ExBs: white arrowheads) or multiple cellular fragments into the perivitelline space of the embryo (ExFs: white arrow). **(b)** A blastocyst with blastomere exclusion immunostained with LAMIN-B1 (green) and γH2A.X (red) using DAPI (blue) for DNA. The large excluded blastomere appeared binucleated with strong γH2A.X signals (top; white arrowhead), indicating that double-stranded DNA breaks had occurred. Brightfield image (below) provided for reference. **(c)** The zona pellucida from the hatched blastocyst that exhibited cellular fragment exclusion with residual DNA positive for DAPI staining (white arrows). **(d)** Additional examples of large excluded blastomeres (white arrowheads; right) collected during the morula-to-blastocyst transition or at the blastocyst stage that were sequenced. CNV plots (left) determined that each excluded blastomere had chaotic aneuploidy. Scale bars: 25 μm. ExB, excluded blastomere. (**e**) Heat map of SNP maternal versus paternal ratios in excluded blastomeres shows various parental origins.

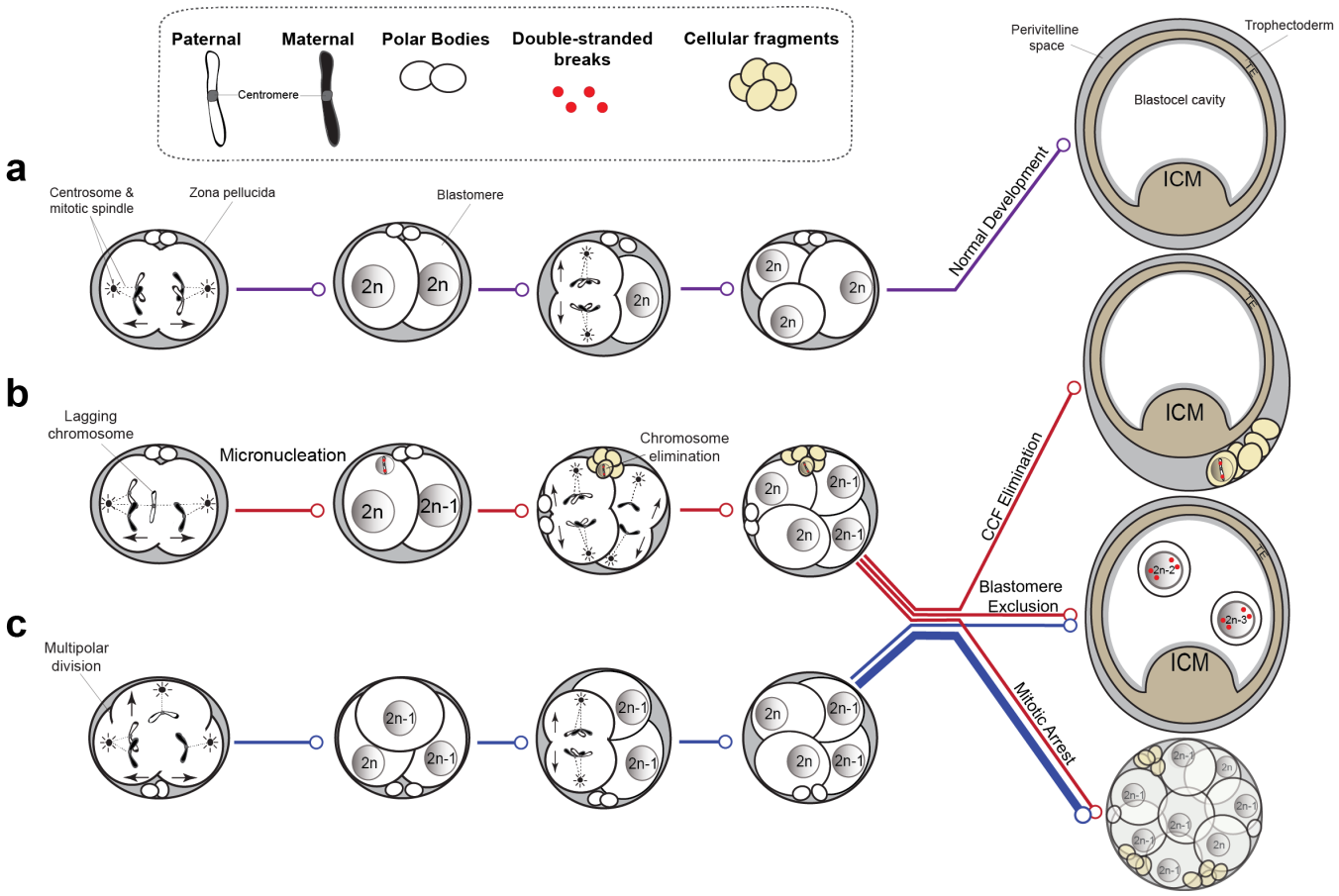

Figure 7. Proposed model of aneuploidy generation and potential resolution in embryos. (a) A simplified model of normal embryo development, whereby a euploid zygote undergoes proper chromosome segregation with cell divisions devoid of cellular fragmentation and blastomere exclusion (purple lines). **(b)** Early embryogenesis of a euploid zygote that contains a lagging chromosome from merotelic attachments during the 1st mitotic division that becomes encapsulated in a micronucleus, where it undergoes DNA damage in the form of double-stranded breaks. Through the process of cellular fragmentation, the damaged chromosome is eliminated from the blastomere and the embryo is most likely to undergo mitotic arrest. However, if the mosaic embryo is able to progress in development to the blastocyst stage, the CCF may be sequestered to the perivitelline space (red lines). **(c)** Abnormal cell divisions, including a tripolar cleavage occurring at the zygote stage, may also generate a mosaic embryo (blue line). The majority of these embryos will be largely aneuploid and eventually arrest when aneuploidy is no longer tolerated and/or a critical number of euploid blastomeres are not achieved (thick blue line). Alternatively, aneuploid blastomeres may still divide beyond embryonic genome activation, but an embryo with severely aneuploid blastomeres that fail to divide will sustain DNA damage and become excluded to the blastocoel cavity upon blastocyst formation.